Synthesis and characterization of sol-gel bioactive glass nanoparticles doped with boron and copper

Synthesis and characterization of sol-gel bioactive glass nanoparticles doped with boron and copper

E. Piatti[1], E. Verné[1], and M. Miola[1*]

[1]Department of Applied Science and Technology, Politecnico di Torino, Turin, Italy

*Corresponding author:
Marta Miola
Department of Applied Science and Technology,
Politecnico di Torino, Torino (TO), Italy
Institute of Materials Engineering and Physics
Corso Duca degli Abruzzi, 24 - 10129 (TORINO) ITALY
Tel: +39 0110904717
Fax: +39 011 0904624
Fax: +39 011 0904624

ABSTRACT

In this work the sol-gel synthesis of bioactive glass nanoparticles containing both boron and copper oxides is reported for the first time in literature. Two acid/base co-catalysed methods were compared. The obtained glasses have been characterized in terms of morphology, composition, particle surface area, phase analysis and bioactivity in acellular simulated body fluids. Almost spherical nanoparticles (< 100 nm diameter), characterized by a certain degree of aggregation and compositions coherent with the theoretical ones, were obtained. Each glass revealed the ability of promote the growth of hydroxyapatite on its surface during soaking in simulated body fluid, assessing that the addition of copper and boron did not negatively affect the bioactivity of the sol-gel derived glasses. Future investigations will be devoted to biological characterizations focused on cytotoxicity, antibacterial properties and pro-angiogenetic ability.

Keywords: Glass, Nanoparticles, Sol-gel, Bioactivity, Copper, Boron

1. Introduction

Bioactive glasses (BGs) are well-known inorganic oxide-based materials able to bind with living tissues and stimulate new tissue growth by reacting with physiologic fluids [1,2]. The *in vivo* bone-bonding capability of BGs can be successfully predicted *in vitro* by soaking in simulated body fluid (SBF) and observing the formation of hydroxyapatite (HA) on their surface, as reported in a variety of studies [2–6]. Therefore, BGs are classified as third generation biomaterial, being biocompatible, bioactive, osteoconductive and even osteoproductive [7,8].

Indeed, the main application field of bioactive glasses is the hard tissue regeneration, with some clinical use in orthopaedics and dentistry [5,9,10]. However, over the years, many new glass compositions with potential applications in hard and soft tissue engineering have been developed, as largely reviewed [5,11–16]. In fact, according to the released ions, BGs dissolution can influence gene expression of cells and/or even display an antibacterial effect [17–19]. Provided that released metallic ions influence signaling pathways and stimulate metabolic effects involved in tissue formation, inducing intracellular and extracellular responses [6], several new BGs compositions have been investigated in literature, reporting the effect of additional elements such as barium [20], boron [21–23], cerium [19,24,25], cobalt [26–28], copper [29–34], fluorine [35], gallium [24,25], iron [20], magnesium [28,29,36], manganese [37–39], potassium [40], silver [41–44], strontium [33,36,45–48], terbium [49], or zinc [22,24,44,50,51]. The result of the addition into bioactive glasses of different metallic ions on their biological performances has been very well reviewed by Hoppe et al. [52].

For both hard and soft tissue regeneration, angiogenesis (the formation of new blood vessels) is fundamental in order to achieve the formation of a new functional and vascularized tissue [53,54]. In this scenario, the development of ion-doped BGs exhibiting angiogenic properties is of primary importance [55]. Boron has been demonstrated to promote angiogenesis [23,56,57] and boron-doped materials have been tested *in vivo* for their wound regeneration potential [54,58]. Recently, copper has shown angiogenic potential as well, as reported by various experimental results [59–62].

Moreover, BGs can contain metallic ions that confer them an antibacterial effect. Indeed, the outbreak of bacterial infections is a relevant problem that can hinder the tissue regeneration and lead to the implant failure. Silver is the most common ion used for the synthesis of antibacterial materials [41–44,63,64], but also other ions, such as copper [30,32,34,62,65,66], have shown antibacterial ability.

So, owing to their angiogenic and antibacterial/antimicrobial properties, BGs containing copper or boron are largely studied, but very few glass compositions (and even less BGs compositions) incorporating both ions have been produced, manly by melting-quenching technique [67–76].

Despite to the quite wide amount of literature concerning Cu-doped glasses, only few of the above cited studies have potential biomedical applications.

Traditionally, BGs have been produced by melting-quenching technique, but since its discovery the sol-gel technique has shown successful results for the synthesis of BGs with various compositions and shapes. The sol-gel process allows the synthesis of solid materials (polymeric, metallic, ceramics or glass materials) from a solution of liquid precursors (sol-state), that undergoes some reactions of hydrolysis and polycondensations and forms a gel. Then, an ageing step and thermal treatments (drying, calcination,

densification) are carried out on the gel, in order to obtain a dense solid material. The detailed explanation of the reactions, synthesis steps, and parameters influencing the synthesis is available in the numerous reviews published on this topic [16,77–81]. The sol-gel synthesis offers many advantages over the melting-quenching one [77,79] such as:

- low processing temperatures
- easy production of glasses with various compositions and different physical and chemical properties
- high control on composition, morphology, and size
- facile and homogeneous doping with metallic ions
- high surface area of the synthesized glasses, which show a high numbers of surface silanols
- higher bioactivity of the sol-gel glasses.

Among the possible structures, nanosized BG particles show very interesting features, such as higher surface area, faster ion release, quicker deposition rate of the hydroxyapatite layer and so higher bioactivity, possibility to enter a cell, accumulating inside the lysosome and delivering their therapeutic ions directly inside the cell [46,82,83]. Moreover, they are considered ideal fillers for tissue engineering scaffolds [2]. On the basis of the author's knowledge of the literature concerning sol-gel synthesis, none of the above cited studies reported the sol-gel route for the preparation of B and Cu doped BGs.

In this scenario, aiming to develop innovative BG compositions for soft tissue engineering applications, in the present paper new B and Cu doped BGs have been synthetized through a very promising sol-gel route. With the attempt to develop an original BG composition

with potential angiogenic and antibacterial properties, the glasses have been prepared starting from the composition of the 77S BG [84], which was modified by the addition of both B and Cu ions, for the first time on the basis of authors knowledge. In order to synthetize small BG nanoparticles, on the basis of previous literature results [78,85,86], two acid/base co-catalysed synthesis methods were adopted and six glasses with three different compositions (wt%) were synthesized, as reported in the Experimental procedure. In brief, our methods are based on the combination of an acid synthesis and the Stöber method. In acid sol-gel syntheses, both hydrolysis and polycondensation reactions take place in acid environment, using acids as catalysts. The acid method is the first ever developed sol-gel synthesis strategy and is largely used for the synthesis of glasses, especially in form of monoliths.[77] The classical Stöber method allows the synthesis of monodisperse spherical silica particles (from 0.05 to 2 μm), from silicon alkoxides precursors (usually tetraorthosilicate, TEOS) in a solution composed of water, alcohol and ammonium hydroxide under continuous agitation [79,87,88], Ammonia is used as catalyst for both hydrolysis and polycondensation reactions that take place during the sol-gel synthesis [87–89]. Up to now, the Stöber method has been used for the synthesis of silica, carbon, TiO_2, bioactive glass and hybrid particles [79,88,90–92]. Our synthesis strategies combine the previous described processes, because the TEOS hydrolysis takes place in acid medium (i.e a solution of ethanol, distilled water and nitric acid) like in a traditional acid synthesis and, in agreement with the Stöber method and previous literature results, the ammonia solution was used in order to reduce the gelation time from hours (or even days) to minutes [93] and induce the accelerated formation of particles [78,87].

Since, as above mentioned, this is the first experimental work based on sol-gel bioactive glasses containing both B and Cu ions for therapeutic application, the present paper is focused on the innovative co-doping, on the optimization of the acid/base co-catalysed synthesis method, and on the evaluation of their influence on the morphology, the particle surface area, the composition and the microstructure of the obtained new sol-gel compositions. Although some compositional changes in bioactive glasses can be easily introduced to give specific added values without hampering their bioactivity (which is the intrinsic rationale of "doping" their composition with small amounts of therapeutic ions) the eventual influence of the doping elements in the bioactivity process of the new glass compositions is not predictable, so it has been also verified for the new BGs developed in this work.

These preliminary work on new co-doped BGs formulation, obtained by unconventional wet route, give new understanding of the fundamental science of BGs and represents an essential starting point for future investigations about the potential synergistic effect of co-doped sol-gel BGs in the field of tissue engineering.

2. Materials and Methods

2.1 Materials

The six glasses with three different compositions (wt%) synthesized in this work can be summarized as follows:

- *S1* and *S2*: 77%SiO_2-9%P_2O_5-14%CaO
- *SB1* and *SB2:* 62%SiO_2-9%P_2O_5-14%CaO-15%B_2O_3
- *SBCu1* and *SBCu2*: 62%SiO_2-9%P_2O_5-9%CaO-5%CuO-15%B_2O_3

where S refers to the silica-based glass network, B to the presence of boron, Cu to the addition of copper and 1 or 2 to the used synthesis route (named synthesis 1 and synthesis 2).

2.2 Bioactive glass synthesis

Aiming to produce small spherical nanoparticles, a previously studied acid synthesis [84,94] was combined with the Stöber method. Thus, the BGs were synthesized by two acid/base co-catalysed synthesis methods, as summarized in Figure 1, using tetraorthosilicate (TEOS) $C_8H_{20}O_4Si$ at 99% (Sigma Aldrich), triethyl phosphate (TEP) $C_6H_{15}O_4P$ at 99% (Alfa Aesar), calcium nitrate tetrahydrate $Ca(NO_3)_2 \cdot 4\ H_2O$, copper nitrate trihydrate $Cu(NO_3)_2 \cdot 3\ H_2O$ (Fluka) and boric acid H_3BO_3 at 99% (Sigma Aldrich) as precursors for SiO_2, P_2O_5, CaO, CuO and B_2O_3, respectively. Bi-distilled water and ethanol (EtOH, Sigma Aldrich) were used as solvents. Nitric acid (HNO_3) at 70% (Sigma Aldrich) and ammonia solution NH_4OH at 28-30% (Emsure) were used as catalysts, hydrolysis catalyst and gelling catalyst, respectively.

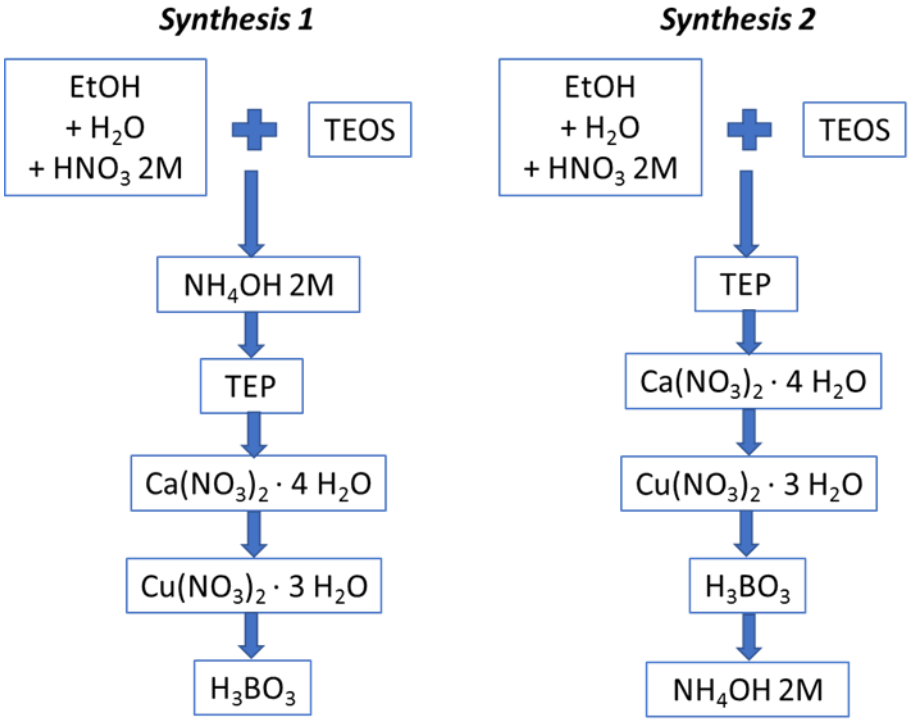

Figure 1: Sol-gel synthesis routes

The difference between the two followed synthesis methods is the addition time of the ammonia solution, which was added dropwise during vigorous magnetic stirring till formation of a gel, characterized by a pH value in the range 8 – 9. In the synthesis 1 the addition of NH_4OH 2M followed the hydrolysis of TEOS and the formation of pure silica nanoparticles in an acid media, whereas in synthesis 2 NH_4OH 2M was added at the end of the synthesis process, after the addition of all precursors. During ammonia solution addition, the pH was carefully monitored. It is well known that the reaction pH influences the size of the final particles [77,79], for example, for silica particles, literature reports a minimum size of 30-80 nm, obtained at a pH value of 9-10 [95]. In both synthesis routes the hydrolysis of TEOS was performed magnetically stirring the silica precursor for 1 h in a mixture of EtOH, H_2O (Milli Q) and HNO_3 (with a molar ratio H_2O+HNO_3: TEOS = 8) and the other precursors were added under gently magnetic stirring at interval time

of 30 min from each other, in agreement with the sequence shown in Figure 1 and the different desired glass compositions. All gels were dried at 60 °C in a heater for 48 h and then calcinated at 700 °C in furnace for 2 h.

2.3 Morphological and compositional characterization

The field emission scanning electron microscope FE-SEM Gemini SUPRATM 40 (Zeiss, Germany), equipped with Energy Dispersion Spectrometry (EDS), was used to perform the morphological (shape and size of the glass particles) and compositional analysis of the samples, which were prepared attaching the glass powders on an aluminium stub using a double-side carbon tape and sputtering them with chromium for 100 s. Depending on the glass type, the particles size was estimated on representative SEM micrographs at 100.00 KX and 150.00 KX.

2.4 BET measurements

The N_2 adsorption and desorption measurements were carried out using the analyser ASAP 2020 Plus (Micrometrics, United States) and the particle surface areas were calculated according to the Brunauer, Emmett, Teller method (called the BET method).

2.5 X-ray diffraction characterization

The X-ray diffraction (XRD) analysis was performed in order to study the glass structure. For the spectra measurements, the X'Pert Philips diffractometer was used, adopting the Bragg Brentano camera geometry and the Cu-Ka incident radiation, with a source voltage of 40 kV, a current of 30 mA, an incident wavelength λ of 1.5405 Å, a step size $\Delta(2\theta)$ of 0.02° and a counting time of 1 s per step. The analysis degree 2θ was varied between 10°

to 70°. The X'Pert HighScore program (equipped with PCPDFWIN database) was used for the spectra analysis.

2.6 FTIR analysis

Fourier Transform Infrared Spectroscopy was carried out on bioactive glass powder samples using the Thermo Scientific Nicolet iS50 FT-IR Spectrometer (equipped with OMNIC software) and KBr pellets (FTIR-KBr). Pellets were produced using 2 mg of glass and 150 mg of KBr, both before and after soaking in SBF. The spectrometer was used in transmission mode with a chosen number of spectral scans equal to 32, a resolution of 4 cm^{-1} and a wavenumber range between 4000 and 525 cm^{-1}.

2.7 Acellular bioactivity test

The *in vivo* bone bonding ability of a BG can be reproduced *in vitro* by soaking the material in simulated body fluid (SBF) and observing the formation of a HA layer on the surface [6]. The SBF is a protein-free and acellular aqueous solution, buffered at physiological pH and characterized by a composition and a concentration of ions, that is similar to those of the inorganic part of human plasma [3]. Therefore, soaking the BGs in the SBF enable to mimic *in vitro* the reactions that occur *in vivo* on the glass surface when the BG is in contact with the human plasma and to study *in vitro* the BG bioactivity. Being these reactions time-dependent [8], two samples of each synthesized glass were soaked in SBF till 14 days, measuring the solution pH after 1, 3, 5, 7, 10, 12 and 14 days and analyzing the glass samples using SEM-EDS, XRD and FTIR at fixed time points (1, 3, 7 and 14 days).

The SBF solution was prepared according to Kokubo protocol,[3] by dissolving NaCl,

KCl, $K_2HPO_4 \cdot 3H_2O$, $MgCl_2 \cdot 6H_2O$, $CaCl_2$, and Na_2SO_4 into distilled water and buffering at pH 7.4 with tris (hydroxymethyl) amminomethane $(HOCH_2)_3CNH_2$ (TRIS) and hydrochloric acid (HCl).

The mass/volume ratio between glass powders and SBF solution was 1:1, so 100 mg of glass were soaked in 100 ml of SBF, in agreement with previous literature experimental works [96]. The glass samples were kept at 37 °C in an orbital shaker (IKA® KS4000i control) with a shaking movement rate of 120 rpm and the SBF was never renewed during all acellular bioactivity test. At each time point, glass powders were removed from SBF, rinsed with deionized water, centrifugated at 5000 rpm for 10 minutes and then dried in an incubator at 37 °C.

3. Results and discussion

3.1 Morphological and compositional characterization

Figure 2 reports the SEM micrograph of SB1 glass as example of the size and morphology obtained for each glass. Round-shaped particles, with size in the nanometric range, were obtained for all syntheses and compositions, with mean particle size of all glasses smaller than 100 nm and a predominant diameter of about 50 nm, confirming that the acid-base co-catalyzed route is a useful procedure for the synthesis of nanosized BG particles [42,51,85,97–101].

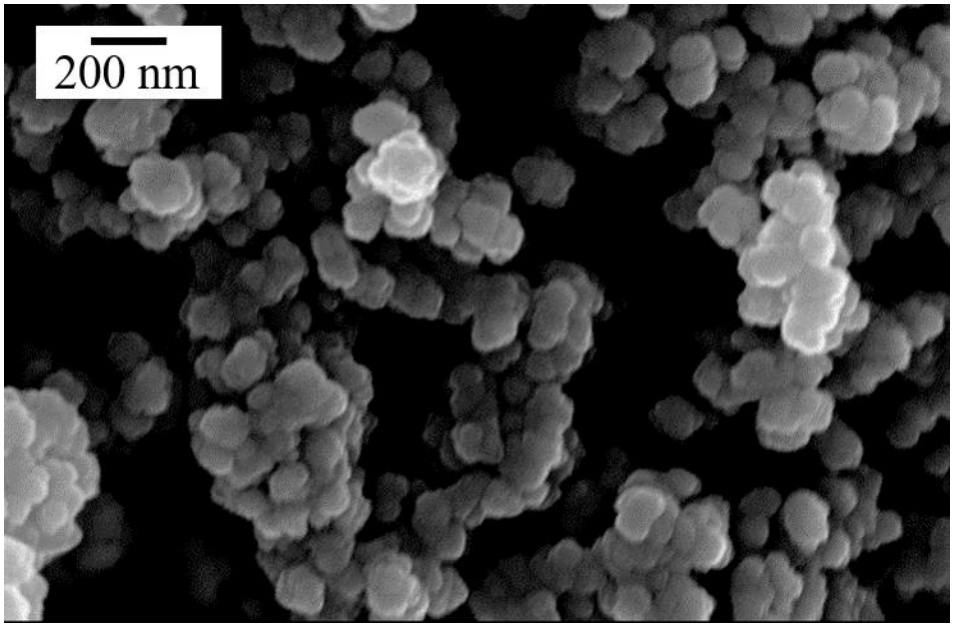

Figure 2: SEM micrograph of SB1 glass

However, all six glasses exhibit a certain degree of aggregation, in agreement with previous literature results. Indeed, because of their high surface area and high surface energy, it is common to observe aggregation in case of nanoparticles [4,19,38,78,102–104]. The different synthesis routes and the doping with B and Cu seem not to affect the final morphology, since any significant change in size and shape among the different glasses were observed, in agreement with literature results showing no morphological variation when doping ions are added into other BGs [44]. Therefore, the main parameter affecting the final particle morphology seems to be the initial hydrolysis of TEOS in an acid environment (pH < 2.5) [81]. Indeed, this acid condition favors the rapid hydrolysis of TEOS, occurring faster than polycondensation, which starts before the complete hydrolysis of the silica precursor, leading to the formation of a large number of Si-O-Si linkages [81]. The addition of P, Ca, B and Cu ions did not alter the pH of the sols, which were acid (with pH values in the range 0.5 – 1.8) till the addition of the ammonia solution, used as gelling agent.

EDS analysis (not reported) confirmed the glasses composition and evidenced that the amount of phosphorus was slightly underestimated if compared to the theoretical composition.

3.2 BET measurements

BET results confirm that the surface area of sol-gel glasses is bigger in comparison to melt-derived glasses [31,33,105]. As reported in other experimental works, the addition of metallic doping elements leads to a decrease in the measured surface area [19,62,65,106,107]. Indeed, in this work it was observed that the B and Cu co-doped glasses (SBCu1 and SBCu2) were characterized by smaller areas, if compared to the other synthesized glass compositions, as shown in Figure 3. Among these two doped glasses, the ones containing copper showed the smallest surface areas in agreement with previous results of Luo et al. [108], who stated that Cu ions could have a negative effect on the condensation of precursors, which led to significant decreases in the specific surface area and pore volume. In agreement with literature [31,109], the addition of doping ions led to an increase in particle aggregation. This could be probably related to particle formation and growth according to the aggregation model of Stöber process, which are based on nucleation of primary particles, aggregation of nucleated solid particles and absorption of smaller particles by larger particles [31,92,110]. The incorporation of doping ions can modify the charge of the system, altering the thermodynamic interactions between the solvent and the hydrolyzed intermediates. Moreover, the metallic ions are only adsorbed on the particle surface and diffuse into the silicate structure upon calcination at high temperature, as previously reported by Zheng et al. [31], thus this metallic ions shell can lead to an increased particle aggregation. Moreover, the surface area of glass nanoparticles obtained by synthesis 1 is bigger in relation to the synthesis 2. This could

be related to the different addition timing of ammonia solution, being well-known that ammonia addition affects the particle dispersion [111].

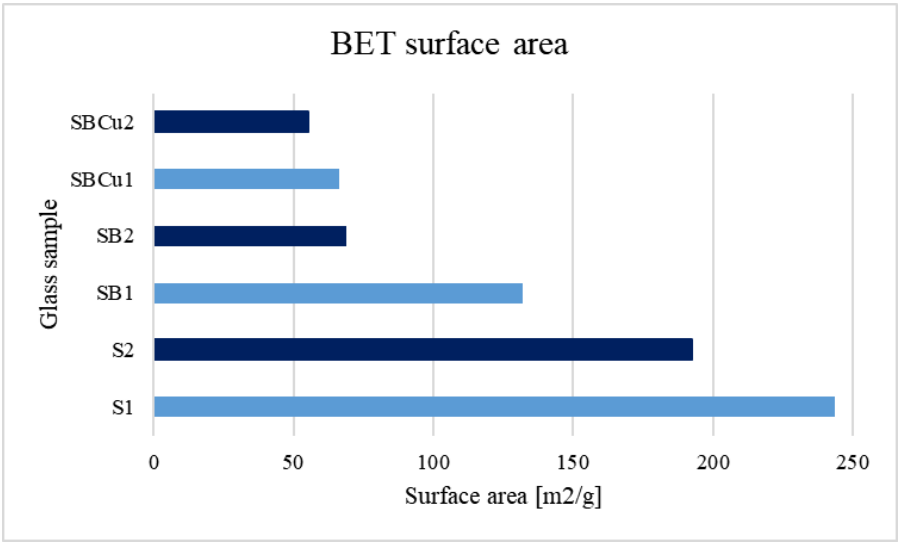

Figure 3: BET surface areas

All thermal isotherms of N_2 adsorption and desorption are reported in

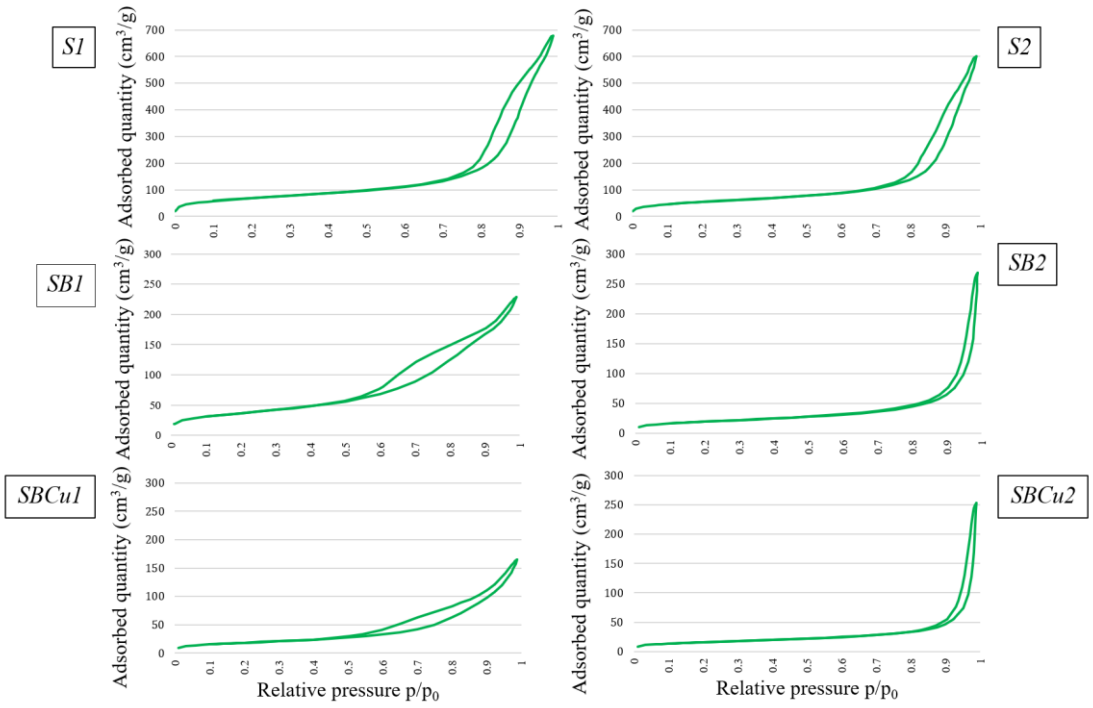

Figure *4*. No significant differences can be observed between isotherms of synthesis 1 and synthesis 2. The isotherms can be identified as type IV according to IUPAC classification [112] and in all of them it is possible to observe a hysteresis loop at high P/P_0 region (starting around 0.7 in case of S1 and S2, around 0.5 in case of SB1 and SBCu2 and around 0.8 in case of SB2 and SBCu2). The hysteresis can be classified as H1 type, according to IUPAC classification and to literature [113].

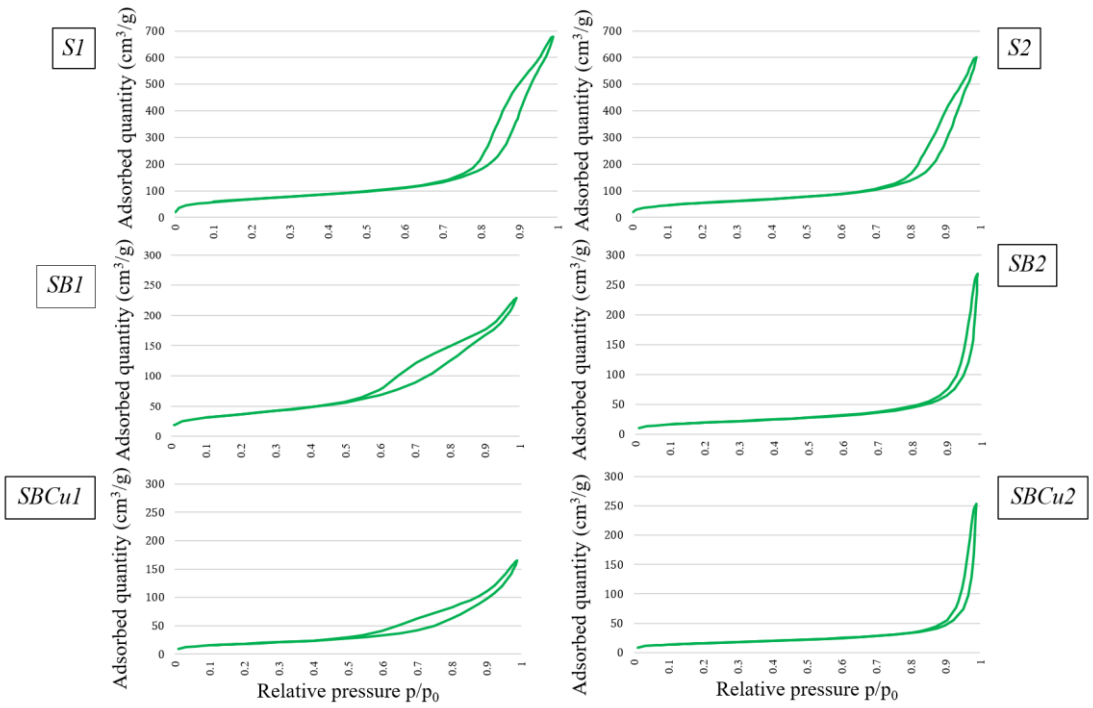

Figure 4: N_2 adsorption and desorption isotherms

This type of isotherm curve is typical of mesoporous materials [37,114,115], but the presence of a hysteresis loop at so high values suggest that the measured mesopores were not related to a mesoporous structure inside the particles (in agreement with the used synthesis method), but derived from the interstitial space among the nanoparticles, as already previously reported by Miao et al. [116].

3.3 X-ray diffraction characterization

The XRD patterns (Figure 5) show the predominant amorphous nature of the samples, as displayed by the broad amorphous halo between 15° and 30° (characteristic of all glassy materials). Three low intensity broad signals at 26°, 32° and 40° respectively are visible in the patterns of the doped glasses (the principal one at 32° is barely visible only in the not doped glasses) and can be attributed to small amounts of a calcium silicate Ca_2SiO_4 (code 00-033-0303) nucleated during the calcination step of the synthesis, as expected in case of sol-gel synthesis of complex compositions [19,117]. No significant differences were observed between the two different synthesis methods.

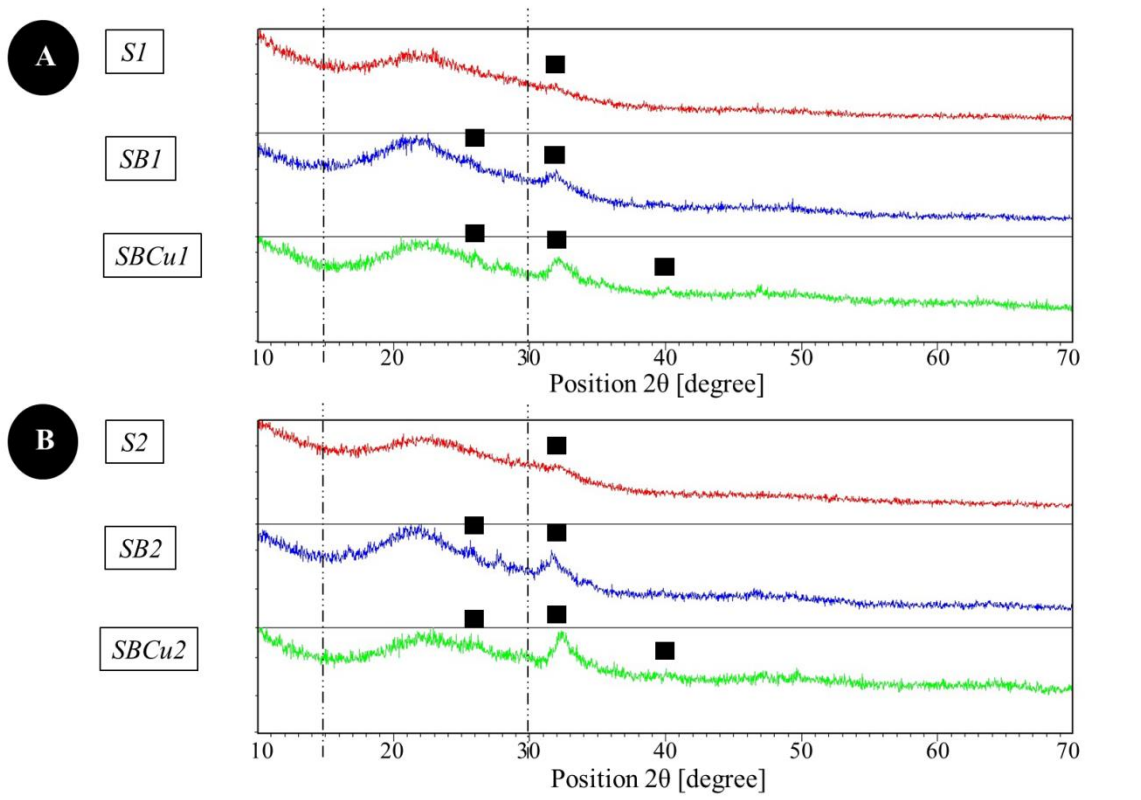

Figure 5: XRD spectra of all six synthesized glasses – A) S1, SB1 and SBCu1 B) S2, SB2 and SBCu2

3.4 FTIR analysis

.

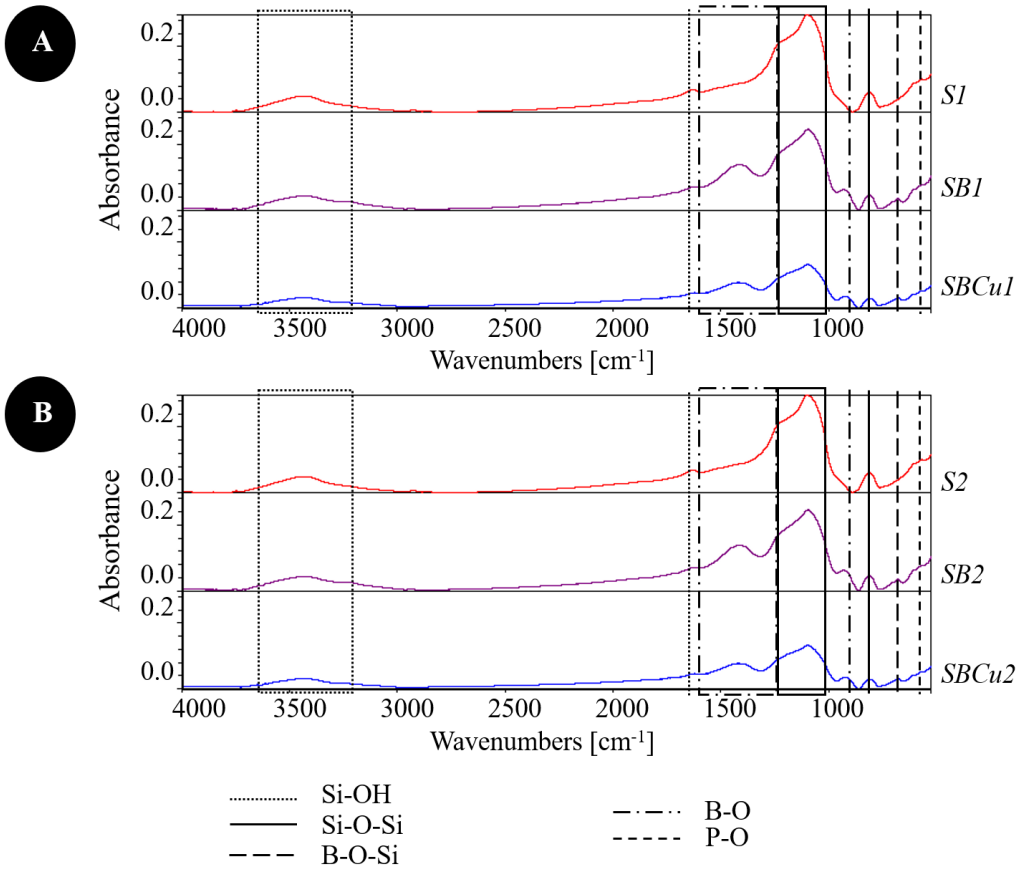

Figure *6* shows the FTIR spectra of the synthesized glasses. In all samples a shoulder between 1000 and 1200 cm^{-1} and two peaks at 800 cm^{-1} and around 600 cm^{-1} were observed. The shoulder between 1000 and 1200 cm^{-1} and the peak at 800 cm^{-1} are typical of a silicate network, in details they characteristic of the Si-O-Si asymmetric [41,42] and symmetric stretching vibration [41,105,118–120], respectively. The peak around 600 cm^{-1} is attributed to P-O-P bending vibrations [41,51,121]. In the FTIR spectra of samples containing boron (SB1, SB2, SBCu1 and SBCu2), additional peaks are clearly visible: a large peak between 1200 cm^{-1} and 1600 cm^{-1} and two smaller peaks at 942 cm^{-1} and at 650 cm^{-1}, that can be attributed to B–O bond stretching vibrations of triangular [BO_3]

elementary units [122,123], B–O bond stretching vibrations of tetrahedral [BO_4] units[124] and borosiloxane bonds [125], respectively. Therefore, the incorporation of boron ions in the BG particles was confirmed. It was not possible to detect vibrations related to Cu–O bond, because they are revealed at wavenumbers lower than 400 cm^{-1}, but the presence of copper inside the glass particles was already confirmed by EDS spectra, where the Cu peak is clearly visible (data non reported) [29].

The hygroscopic nature of these glasses is revealed the presence of a broad band between 3600 and 3375 cm^{-1} and a peak at 1653 cm^{-1}, which can be ascribed to the SiO-H stretching vibrations of bond between the hydrogens of the surface silanols and water (SiO-H···H_2O) [126].

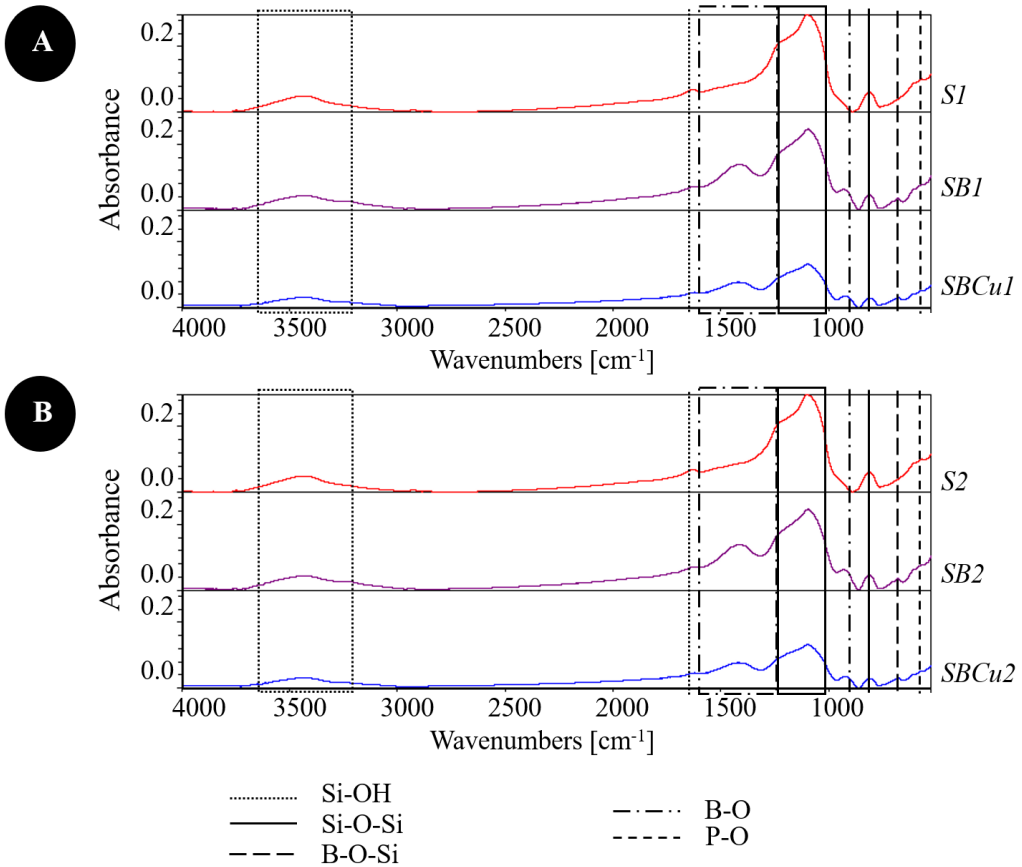

Figure 6: FTIR spectra of all six synthesized glasses – A) S1, SB1 and SBCu1 B) S2, SB2 and SBCu2

3.5 Acellular bioactivity test

HA formation on a material surfaces upon immersion in SBF is considered a qualitative measure of its bioactivity [1,127]. As explained by Hench et al. [8,9], when in contact with SBF or biologic fluids, the BG partially dissolves and exchanges alkali ions with hydrogen ions from body fluids, leading initially to a certain pH increase, then to the formation of silica gel on the BG surface and later to the deposition of a biologically reactive hydroxy-carbonate apatite.

With time, the interfacial HA layer continues to grow by incorporating calcium and phosphorus ions from body fluids [8]. Therefore, as expected, EDS patterns and plots of ions amounts versus soaking time in SBF (.

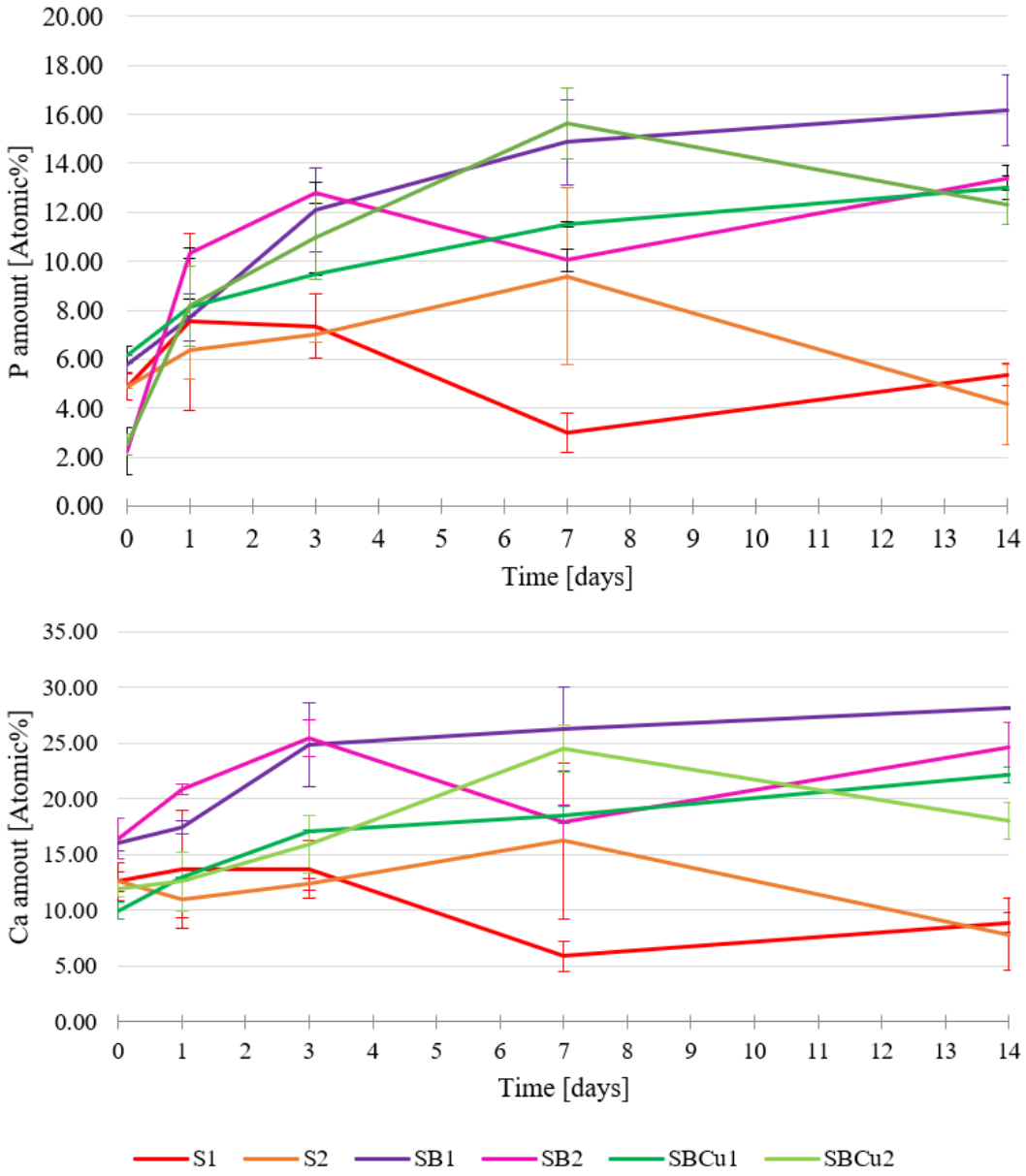

Figure *7*) show an increase in P and Ca amounts on the surface of the synthesized glasses during immersion in SBF. The Ca/P atomic ratios (calculated from the EDS results over three spectra) were similar to the ratio value of stoichiometric hydroxyapatite (1.67) as reported in Table 1 [128,129].

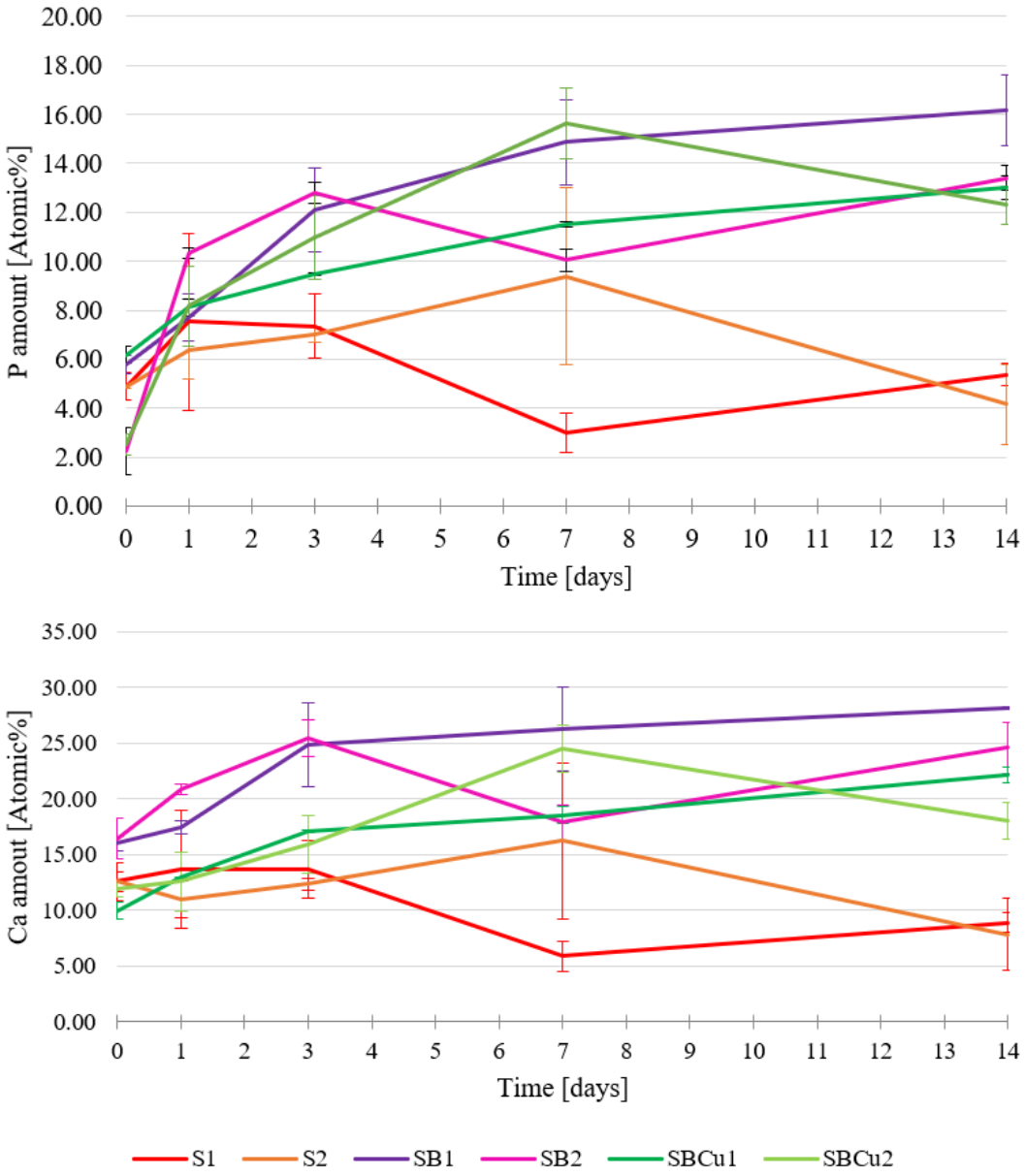

Figure 7: Amounts of P and Ca ions versus soaking time in SBF. The analyses were performed on three spectra for each glass composition.

Ca/P ratio (atomic%)				
Glass	1d	3d	7d	14d
S1	1.81	1.86	1.95	1.65

S2	1.72	1.76	1.73	1.87
SB1	2.26	1.77	1.77	1.74
SB2	2.01	1.78	1.78	1.83
SBCu1	1.60	1.80	1.61	1.70
SBCu2	1.54	1.45	1.56	1.47

Table 1. Ca/P atomic ratios (calculated from the EDS results) versus soaking time in SBF

Solution pH values versus soaking time (reported in Figure *8*) did not show any important variation up to 14 days. In fact, the measured pH varied only in the range 7.34–7.56 during all soaking time, showing a slight increase by increasing immersion time, as expected for the early stage bioactivity mechanism. To better underline this slowly increasing trend the tendency line of pH values is reported in case of S2 sample.

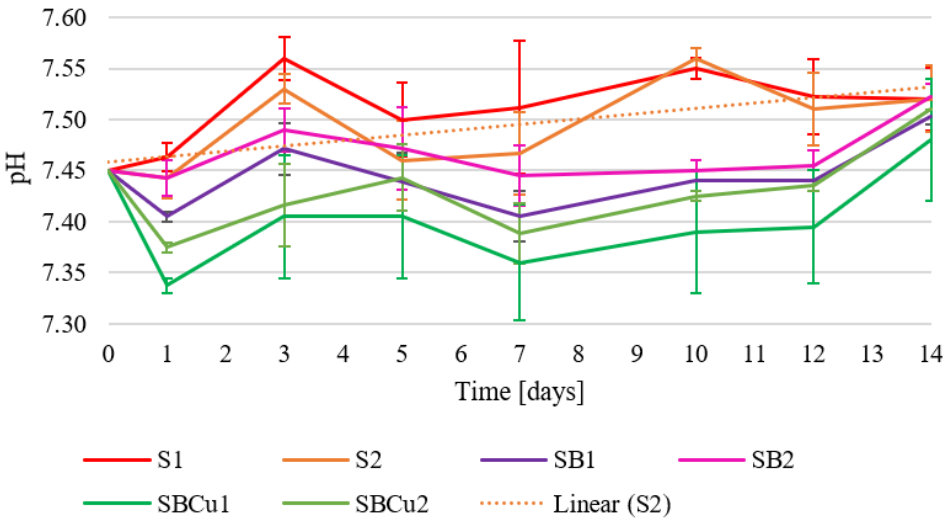

Figure 8: Solution pH versus soaking time in SBF

The fluctuations in pH trends can be attributed to ion exchange between the SBF solution and the glass powders, in agreement with other experimental results [130]. Trends of B-containing glasses (SB1 and SB2) seems to be flatter and lower, probably due to the

buffering effect of boron [131]. The lowest pH values are shown by glasses containing copper (SBCu1 and SBCu2) [30]. The pH trend is slightly shifted to lower values for the different type of glass in this way: S > SB > SBCu. Anyway, it must be underlined that the differences among the three synthesized compositions are very small. Finally, it is worth of mention that the measured pH values were suitable for cell adhesion and proliferation being 6.5–7.8 the recommended appropriate pH range for the adhesion and proliferation of cells [132–134].

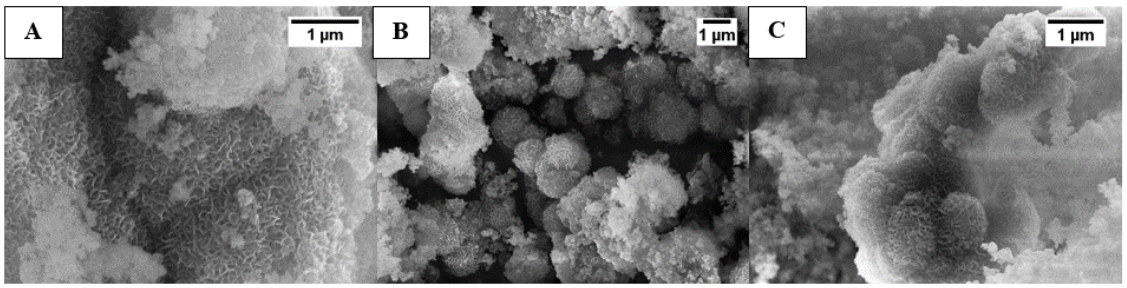

Figure 9: SEM micrographs of glasses of synthesis 2 after 14 days of immersion in SBF – A) S2 B) SB2 C) SBCu2

From SEM micrographs, recorded after 14 days of immersion in SBF, it is possible to see that the glass surface is totally covered by a hydroxyapatite layer. In

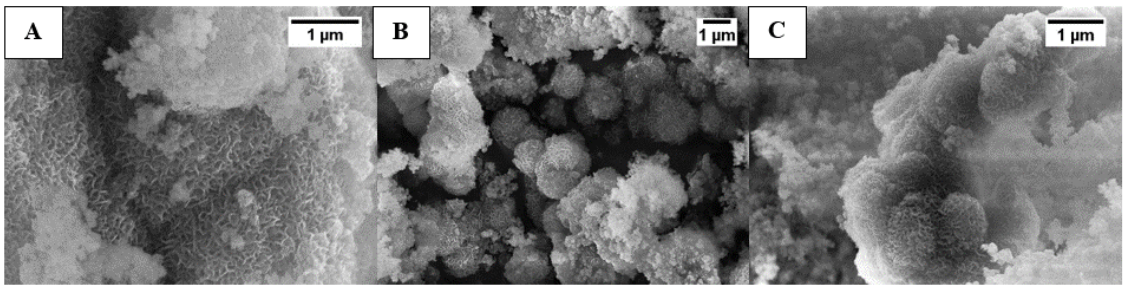

Figure 9, the rough and cauliflower-like morphology typical of HA crystals on S2, SB2 and SBCu2 is shown as example.

The evolution of the XRD peaks of all samples during all acellular bioactivity test is reported in figure 10, in order to provide a comparison between the rate of hydroxyapatite formation of the different synthetized glasses and to underline, if any, eventual differences among the samples. After immersion in SBF, in the XRD patterns, reported

in Figure 10, new peaks appear, that can be attributed to hydroxyapatite (code 00-001-1008), showing that the synthesized glasses are bioactive, since the first day of immersion in SBF. Moreover, peaks related to the calcium silicate crystalline phase, also corresponding to peaks attributable to HA, appear more intense. Regarding the peak intensity, it should be also observed that in some XRD spectra the presence of NaCl could be detected. It arose from SBF and was not eliminated during the washing step with bi-distilled water, as already experienced in case of BG particles immersed in SBF [135]. Thus, the partial crystallization of the BGNs did not hinder their bioactivity. Moreover the results of the bioactivity test underline that the contemporaneously introduction of B and Cu did not significantly modify the bioactive behaviour of the BGs developed in this work, i.e. it did not affect their ability of inducing HA precipitation into acellular SBF, as instead observed by other authors for glass containing only copper [136]. Thus, the peculiar property of the BGs has been maintained, as their composition has been properly modified introducing small amounts of therapeutic ions without hindering their bioactivity.

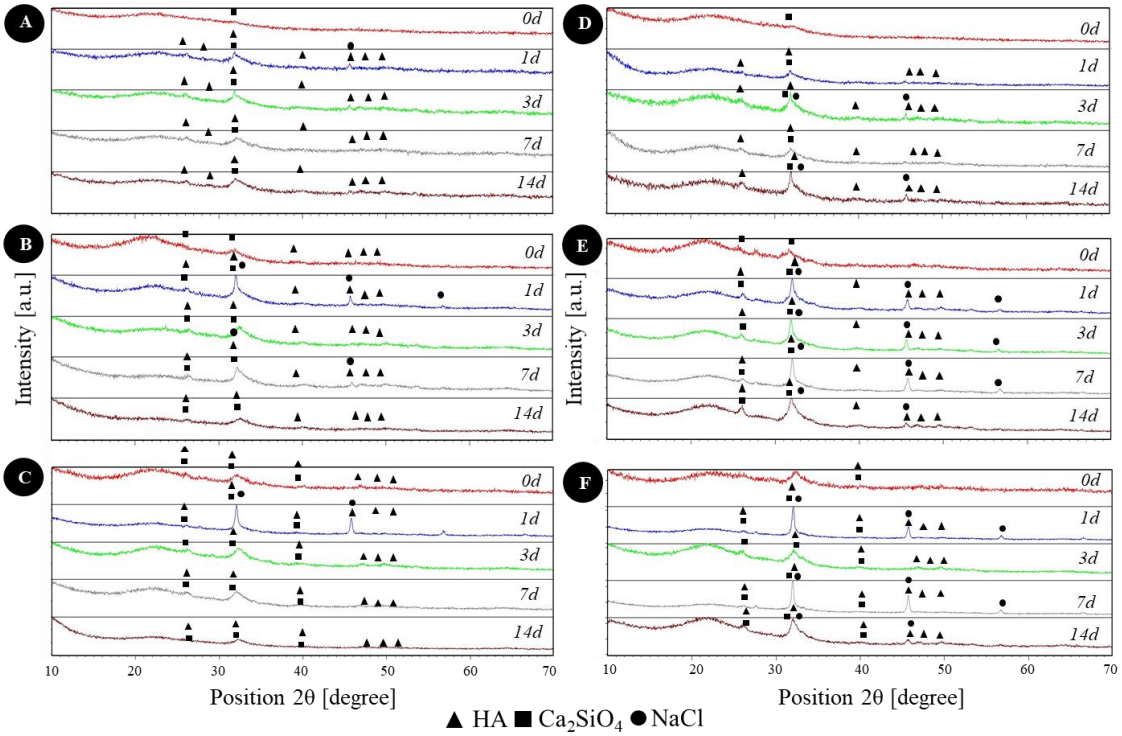

Figure 10: XRD spectra of glasses immersed in SBF at different time points (0d, 1d, 3d, 7d, 14d, ordered from top to bottom of the image) – A) S1 B) S2 C) SB1 D) SB2 E) SBCu1 F) SBCu2

The samples immersed up to 14 days were also analysed using FTIR (Figure 11 and Figure 12), confirming that a HA layer grows on the glass surface during the acellular bioactivity test. After immersion in SBF, the broad band between 3600 and 3375 cm^{-1}, that was seen before immersion in SBF, appears much higher and wider, reaching value around 2700 cm^{-1} and being centred around 3500 cm^{-1}, a peak which can be attributed to the stretching mode of hydrogen-bonded OH^- ions of hydroxyapatite [120]. Two small peaks appear between 1500 and 1300 cm^{-1} and they can be related to the presence of the carbonate groups of carbonated apatite [137,138]. Moreover, the peak around 600 cm^{-1}

[120] and the peaks between 600 and 525 cm^{-1} [19,116,120], previously observed in samples before immersion in SBF and attributed to the vibration modes of the P-O groups, shown an increased intensity after immersion in SBF and thus can be related to an increase in the numbers of P-O groups in the glasses and consequently to the formation of HA. Also, in this case, no evident differences can be observed among the three different compositions and the two syntheses, confirming that all synthesized BGs are bioactive and that the B and Cu insertion did not modify the glass ability to induce the precipitation of HA.

The fact that these B and Cu doped glasses are still bioactive despite the incorporation of metallic doping ions is a not foregone and encouraging result, supporting the hypothesis that our novel biomaterials can take advantages of both their bioactivity and the multifunctional (antibacterial, angiogenic and osteogenic) properties of their doping ions.

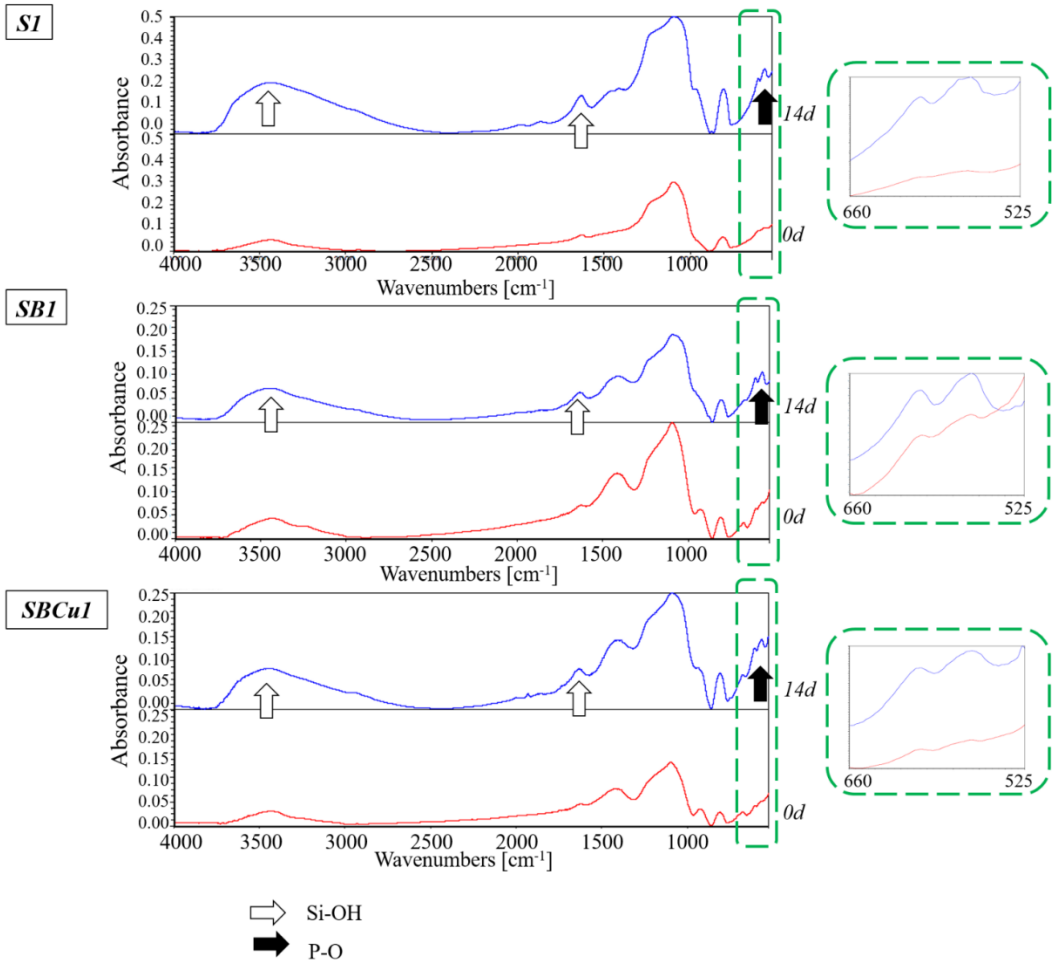

Figure 11: FTIR spectra of synthesis1-glasses before immersion in SBF and after 14 days in SBF

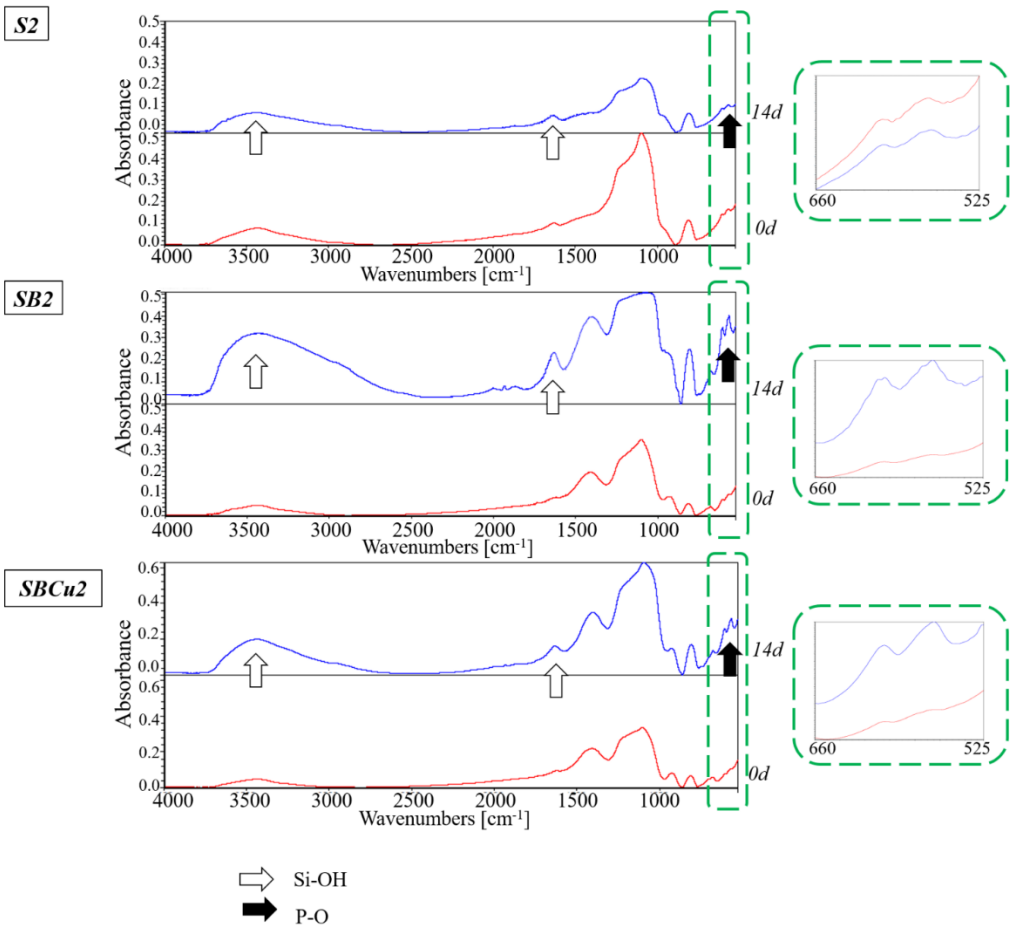

Figure 12: FTIR spectra of synthesis2-glasses before immersion in SBF and after 14 days in SBF

4. Conclusions

The aim of the present work was to design innovative silica-based bioactive glasses co-doped with boron and copper as, using two modified Stöber methods, in particular two acid/base co-catalysed synthesis routes. In both cases, in agreement with previous literature, the ammonia solution was used in order to reduce the gelation time, accelerating the formation of nanosized particles (< 100 nm) with almost spherical shape. A certain degree of aggregation was recorded in both cases. Indeed, the high surface area (detected by BET analysis) of the nanoparticles led them to aggregate. The aggregation

phenomena were more significant for the glass compositions modified with doping elements, since the incorporation of doping ions can modify the charge of the system.

All the obtained glasses revealed a predominantly amorphous nature and a certain tendency to carbonation, which was not hindered by the presence of the small amounts of crystalline phase in the glassy matrix. The glass nanoparticles are able to induce the precipitation of HA *in vitro*, by soaking in SBF, also after co-doping, so they can have potential applications in the tissue engineering field. Any significant difference between the two syntheses and among all glasses was observed on bioactivity kinetics by XRD, FESEM and FTIR analyses.

Nowadays, the synthesis of well dispersed nanosized particles is in fact still challenging. In order to avoid particle aggregation, further optimisation of the synthesis processes is needed, for example varying the type of solvent, the amount of added ammonia solution and the mixing strategy.

Moreover, the co-doping with different ions is believed to be a very successful strategy to modulate cell response, stimulating regeneration of healthy and functional tissues, but it is still a new strategy and the synergic effect of the two doping ions with similar or complementary properties, especially in case of boron and copper, needs further in-depth investigation. Thus, in future works biological characterization will be performed on the optimized samples to assess biocompatibility, antibacterial and pro-angiogenetic properties, in view of their final application.

References

[1] A.R. Boccaccini, J.J. Blaker, Bioactive composite materials for tissue

engineering scaffolds, Expert Rev. Med. Devices. 2 (2005) 303–317. https://doi.org/10.1586/17434440.2.3.303.

[2] Q. Chen, J.A. Roether, A.R.R. Boccaccini, Tissue engineering scaffolds from bioactive glass and composite materials, in: & F.C.© Eds. N Ashammakhi, R Reis (Ed.), Top. Tissue Eng., 2008: p. 27.

[3] T. Kokubo, H. Takadama, How useful is SBF in predicting in vivo bone bioactivity?, Biomaterials. 27 (2006) 2907–2915. https://doi.org/10.1016/j.biomaterials.2006.01.017.

[4] G.M. Luz, J.F. Mano, Preparation and characterization of bioactive glass nanoparticles prepared by sol–gel for biomedical applications, Nanotechnology. 22 (2011) 1–11. https://doi.org/10.1088/0957-4484/22/49/494014.

[5] L. Gerhardt, A.R. Boccaccini, Bioactive Glass and Glass-Ceramic Scaffolds for Bone Tissue Engineering, Materials. 3 (2010) 3867–3910. https://doi.org/10.3390/ma3073867.

[6] K. Rezwan, Q.Z. Chen, J.J. Blaker, A.R. Boccaccini, Biodegradable and bioactive porous polymer/inorganic composite scaffolds for bone tissue engineering, Biomaterials. 27 (2006) 3413–3431. https://doi.org/10.1016/j.biomaterials.2006.01.039.

[7] P. Sepulveda, L.L. Hench, Bioactive hierarchical structures for genetic control of bone morphogenesis, Mater. Res. 5 (2002) 243–246. https://doi.org/https://doi.org/10.1590/S1516-14392002000300004.

[8] L.L. Hench, Bioceramics, J. Am. Ceram. Soc. 81 (1998) 1705–1728.

[9] L.L. Hench, J.M. Polak, Third-generation biomedical materials, Science (80-.). 295 (2002) 1014–1017. https://doi.org/DOI: 10.1126/science.1067404.

[10] L. Tan, X. Yu, P. Wan, K. Yang, Biodegradable materials for bone repairs: A review, J. Mater. Sci. Technol. 29 (2013) 503–513. https://doi.org/10.1016/j.jmst.2013.03.002.

[11] V. Miguez-Pacheco, L.L. Hench, A.R. Boccaccini, Bioactive glasses beyond bone and teeth: Emerging applications in contact with soft tissues, Acta Biomater. 13 (2015) 1–15. https://doi.org/10.1016/j.actbio.2014.11.004.

[12] S. Kargozar, F. Baino, S. Hamzehlou, R.G. Hill, M. Mozafari, Bioactive glasses entering the mainstream, Drug Discov. Today. 23 (2018) 1700–1704. https://doi.org/10.1016/j.drudis.2018.05.027.

[13] M. Erol-Taygun, K. Zheng, A.R. Boccaccini, Nanoscale Bioactive Glasses in Medical Applications, Int. J. Appl. Glas. Sci. 148 (2013) 136–148. https://doi.org/10.1111/ijag.12029.

[14] S. Kargozar, S. Hamzehlou, F. Baino, Potential of bioactive glasses for cardiac and pulmonary tissue engineering, Materials. 10 (2017) 1–17. https://doi.org/10.3390/ma10121429.

[15] F. Baino, G. Novajra, V. Miguez-Pacheco, A.R. Boccaccini, C. Vitale-Brovarone, Bioactive glasses: Special applications outside the skeletal system, J. Non. Cryst. Solids. 432 (2016) 15–30.

https://doi.org/10.1016/j.jnoncrysol.2015.02.015.

[16] L.L. Hench, Sol-gel materials for bioceramic applications, Curr. Opin. Solid State Mater. Sci. 2 (1997) 604–610. https://doi.org/https://doi.org/10.1016/S1359-0286(97)80053-8.

[17] J.S. Fernandes, P. Gentile, R.A. Pires, R.L. Reis, P. V Hatton, Multifunctional bioactive glass and glass-ceramic biomaterials with antibacterial properties for repair and regeneration of bone tissue, Acta Biomater. 59 (2017) 2–11. https://doi.org/10.1016/j.actbio.2017.06.046.

[18] S. Kaya, M. Cresswell, A.R. Boccaccini, Mesoporous silica-based bioactive glasses for antibiotic-free antibacterial applications, Mater. Sci. Eng. C. 83 (2018) 99–107. https://doi.org/10.1016/j.msec.2017.11.003.

[19] Y. Goh, A.Z. Alshemary, M. Akram, A.R.M. Kadir, R. Hussain, In-vitro characterization of antibacterial bioactive glass containing ceria, Ceram. Int. 40 (2014) 729–737. https://doi.org/10.1016/j.ceramint.2013.06.062.

[20] A. Yazdanpanah, F. Moztarzadeh, Synthesis and characterization of Barium – Iron containing magnetic bioactive glasses: The effect of magnetic component on structure and in vitro bioactivity, Colloids Surfaces B Biointerfaces. 176 (2019) 27–37. https://doi.org/10.1016/j.colsurfb.2018.12.036.

[21] B. Gupta, J.B. Papke, A. Mohammadkhah, E.D. Delbert, A.B. Harkins, Effects of Chemically Doped Bioactive Borate Glass on Neuron Regrowth and Regeneration, Ann. Biomed. Eng. 44 (2016) 3468–3477. https://doi.org/10.1007/s10439-016-1689-0.

[22] S.S. Seyedmomeni, M. Naeimi, M. Raz, J. Aghazadeh Mohandesi, F. Moztarzadeh, F. Baghbani, M. Tahriri, Synthesis, Characterization and Biological Evaluation of a New Sol-Gel Derived B and Zn-Containing Bioactive Glass: In Vitro Study, Silicon. 10 (2018) 197–203. https://doi.org/10.1007/s12633-016-9414-z.

[23] P. Balasubramanian, T. Büttner, V.M. Pacheco, A.R. Boccaccini, Boron-containing bioactive glasses in bone and soft tissue engineering, J. Eur. Ceram. Soc. 38 (2018) 855–869. https://doi.org/10.1016/j.jeurceramsoc.2017.11.001.

[24] A.J. Salinas, S. Shruti, G. Malavasi, L. Menabue, M. Vallet-Regí, Substitutions of cerium, gallium and zinc in ordered mesoporous bioactive glasses, Acta Biomater. 7 (2011) 3452–3458. https://doi.org/10.1016/j.actbio.2011.05.033.

[25] A.M. Deliormanli, Electrospun cerium and gallium-containing silicate based 13-93 bioactive glass fibers for biomedical applications, Ceram. Int. 42 (2016) 897–906. https://doi.org/10.1016/j.ceramint.2015.09.016.

[26] C. Wu, Y. Zhou, W. Fan, P. Han, J. Chang, J. Yuen, M. Zhang, Hypoxia-mimicking mesoporous bioactive glass scaffolds with controllable cobalt ion release for bone tissue engineering, Biomaterials. 33 (2012) 2076–2085. https://doi.org/10.1016/j.biomaterials.2011.11.042.

[27] B.R. Barrioni, A.G.S. de Laia, T.M. Valverde, T.M. de M. Martins, M.V. Caliari, M.A. de Sá, A.M. de Goes, M. de M. Pereira, Evaluation of in vitro and in vivo biocompatibility and structure of cobalt-releasing sol-gel bioactive glass, Ceram. Int. 44 (2018) 20337–20347. https://doi.org/10.1016/j.ceramint.2018.08.022.

[28] A. Hoppe, B. Jokic, D. Janackovic, T. Fey, P. Greil, S. Romeis, J. Schmidt, W. Peukert, J. Lao, E. Jallot, A.R. Boccaccini, Cobalt-Releasing 1393 Bioactive Glass-Derived Scaffolds for Bone Tissue Engineering Applications, Appl. Mater. Interfaces. 6 (2014) 2865–2877. https://doi.org/10.1021/am405354y.

[29] V. Giannoulatou, G.S. Theodorou, T. Zorba, E. Kontonasaki, L. Papadopoulou, N. Kantiranis, K. Chrissa, G. Zachariadis, K.M. Paraskevopoulos, Magnesium calcium silicate bioactive glass doped with copper ions; synthesis and in vitro bioactivity characterization, J. Non. Cryst. Solids. 500 (2018) 98–109. https://doi.org/10.1016/j.jnoncrysol.2018.06.037.

[30] R. Koohkan, T. Hooshmand, M. Tahriri, D. Mohebbi-Kalhori, Synthesis, characterization and in vitro bioactivity of mesoporous copper silicate bioactive glasses, Ceram. Int. 44 (2018) 2390–2399. https://doi.org/10.1016/j.ceramint.2017.10.208.

[31] K. Zheng, X. Dai, M. Lu, N. Hüser, N. Taccardi, A.R. Boccaccini, Synthesis of copper-containing bioactive glass nanoparticles using a modified Stöber method for biomedical applications, Colloids Surfaces B Biointerfaces. 150 (2017) 159–167. https://doi.org/10.1016/j.colsurfb.2016.11.016.

[32] H. Palza, B. Escobar, J. Bejarano, D. Bravo, M. Diaz-Dosque, J. Perez, Designing antimicrobial bioactive glass materials with embedded metal ions synthesized by the sol–gel method, Mater. Sci. Eng. C. 33 (2013) 3795–3801. https://doi.org/10.1016/j.msec.2013.05.012.

[33] A. Bari, G. Molino, S. Fiorilli, C. Vitale-Brovarone, Novel multifunctional

strontium-copper co-substituted mesoporous bioactive particles, Mater. Lett. 223 (2018) 37–40. https://doi.org/10.1016/j.matlet.2018.04.006.

[34] M. Miola, E. Verné, Bioactive and Antibacterial Glass Powders Doped with Copper by Ion-Exchange in Aqueous Solutions, Materials. 9(6) (2016) 1–16. https://doi.org/10.3390/ma9060405.

[35] V. Aina, L. Bertinetti, G. Cerrato, M. Cerruti, G. Lusvardi, G. Malavasi, C. Morterra, L. Tacconi, L. Menabue, On the dissolution / reaction of small-grain Bioglass ® 45S5 and F-modified bioactive glasses in artificial saliva (AS), Appl. Surf. Sci. 257 (2011) 4185–4195. https://doi.org/10.1016/j.apsusc.2010.12.019.

[36] D. Bellucci, A. Sola, R. Salvatori, A. Anesi, L. Chiarini, V. Cannillo, Role of magnesium oxide and strontium oxide as modifiers in silicate-based bioactive glasses: Effects on thermal behaviour, mechanical properties and in-vitro bioactivity, Mater. Sci. Eng. C. 72 (2017) 566–575. https://doi.org/10.1016/j.msec.2016.11.110.

[37] B.R. Barrioni, E. Norris, L. Siwei, P. Naruphontjirakul, J.R. Jones, M. de M. Pereira, Osteogenic potential of sol–gel bioactive glasses containing manganese, J. Mater. Sci. Mater. Med. 30 (2019) 1–15. https://doi.org/10.1007/s10856-019-6288-9.

[38] Q. Nawaz, U.A.M. Rehman, A. Burkovski, J. Schmidt, A.M. Beltrán, A. Shahid, N.K. Alber, W. Peukert, A.R. Boccaccini, Synthesis and characterization of manganese containing mesoporous bioactive glass nanoparticles for biomedical applications, J. Mater. Sci. Mater. Med. 5 (2018) 29–64.

https://doi.org/10.1007/s10856-018-6070-4.

[39] M. Miola, C. Vitale-Brovarone, G. Maina, F. Rossi, L. Bergandi, D. Ghigo, S. Saracino, M. Maggiora, R.A. Canuto, G. Muzio, E. Verné, In vitro study of manganese-doped bioactive glasses for bone regeneration, Mater. Sci. Eng. C. 38 (2014) 107–118. https://doi.org/10.1016/j.msec.2014.01.045.

[40] D. Bellucci, V. Cannillo, G. Ciardelli, P. Gentile, A. Sola, Potassium based bioactive glass for bone tissue engineering, Ceram. Int. 36 (2010) 2449–2453. https://doi.org/10.1016/j.ceramint.2010.07.009.

[41] A.A. El-Rashidy, G. Waly, A. Gad, A.A. Hashem, P. Balasubramanian, S. Kaya, A.R. Boccaccini, I. Sami, Preparation and in vitro characterization of silver-doped bioactive glass nanoparticles fabricated using a sol-gel process and modified Stöber method, J. Non. Cryst. Solids. 483 (2018) 26–36. https://doi.org/10.1016/j.jnoncrysol.2017.12.044.

[42] A.M. El-Kady, A.F. Ali, R.A. Rizk, M.M. Ahmed, Synthesis, characterization and microbiological response of silver doped bioactive glass nanoparticles, Ceram. Int. 38 (2012) 177–188. https://doi.org/10.1016/j.ceramint.2011.05.158.

[43] H. Zhu, C. Hu, F. Zhang, X. Feng, J. Li, T. Liu, J. Chen, J. Zhang, Preparation and antibacterial property of silver-containing mesoporous 58S bioactive glass, Mater. Sci. Eng. C. 42 (2014) 22–30. https://doi.org/10.1016/j.msec.2014.05.004.

[44] M. Sadegh, N. Shahrbabak, F. Sharifianjazi, D. Rahban, A. Salimi, A Comparative Investigation on Bioactivity and Antibacterial Properties of Sol-Gel Derived 58S Bioactive Glass Substituted by Ag and Zn, Silicon. 11 (2019) 2741–

2751.

[45] J.S. Fernandes, P. Gentile, M. Martins, N.M. Neves, C. Miller, A. Crawford, R.A. Pires, P. Hatton, R.L. Reis, Reinforcement of poly-L-lactic acid electrospun membranes with strontium borosilicate bioactive glasses for bone tissue engineering, Acta Biomater. 44 (2016) 168–177. https://doi.org/10.1016/j.actbio.2016.08.042.

[46] P. Naruphontjirakul, S.L. Greasley, S. Chen, A.E. Porter, J.R. Jones, Monodispersed strontium containing bioactive glass nanoparticles and MC3T3-E1 cellular response, Biomed. Glas. 2 (2016) 72–81. https://doi.org/10.1515/bglass-2016-0009.

[47] S. Fiorilli, G. Molino, C. Pontremoli, G. Iviglia, E. Torre, C. Cassinelli, M. Morra, C. Vitale-Brovarone, The Incorporation of Strontium to Improve Bone-Regeneration Ability of Mesoporous Bioactive Glasses, Materials. 11 (2018) 2–18. https://doi.org/10.3390/ma11050678.

[48] S. Solgi, M. Khakbiz, M. Shahrezaee, A. Zamanian, M. Tahriri, S. Keshtkari, M. Raz, K. Khoshroo, S. Moghadas, A. Rajabnejad, Synthesis, characterization and in vitro biological evaluation of sol-gel derived Sr-containing nano bioactive glass, Silicon. 9 (2017) 535–542. https://doi.org/10.1007/s12633-015-9291-x.

[49] X. Wang, Y. Zhang, C. Lin, W. Zhong, Sol-gel derived terbium-containing mesoporous bioactive glasses nanospheres: In vitro hydroxyapatite formation and drug delivery, Colloids Surfaces B Biointerfaces. 160 (2017) 406–415. https://doi.org/10.1016/j.colsurfb.2017.09.051.

[50] V. Aina, F. Bonino, C. Morterra, M. Miola, C.L. Bianchi, G. Malavasi, M. Marchetti, V. Bolis, Influence of the chemical composition on nature and activity of the surface layer of Zn-substituted sol-gel (bioactive) glasses, J. Phys. Chem. 115 (2011) 2196–2210. https://doi.org/10.1021/jp1101708.

[51] Y.-F. Goh, A.Z. Alshemary, M. Akram, M.R.A. Kadir, R. Hussain, In vitro study of nano-sized zinc doped bioactive glass, Mater. Chem. Phys. 137 (2013) 1031–1038. https://doi.org/10.1016/j.matchemphys.2012.11.022.

[52] A. Hoppe, N.S. Güldal, A.R. Boccaccini, A review of the biological response to ionic dissolution products from bioactive glasses and glass-ceramics, Biomaterials. 32 (2011) 2757–2774. https://doi.org/10.1016/j.biomaterials.2011.01.004.

[53] S. Kargozar, F. Baino, S. Hamzehlou, R.G. Hill, M. Mozafari, Bioactive glasses: Sprouting angiogenesis in tissue engineering, Trends Biotechnol. 36 (2018) 430–444. https://doi.org/10.1016/j.tibtech.2017.12.003.

[54] Q. Yang, S. Chen, H. Shi, H. Xiao, Y. Ma, In vitro study of improved wound-healing effect of bioactive borate-based glass nano- / micro- fibers, Mater. Sci. Eng. C. 55 (2015) 105–117. https://doi.org/10.1016/j.msec.2015.05.049.

[55] S. Kargozar, S. Hamzehlou, F. Baino, Can bioactive glasses be useful to accelerate the healing of epithelial tissues?, Mater. Sci. Eng. C. 97 (2019) 1009–1020. https://doi.org/10.1016/j.msec.2019.01.028.

[56] L. Bi, M.N. Rahaman, D.E. Day, Z. Brown, C. Samujh, X. Liu, A. Mohammadkhah, V. Dusevich, J.D. Eick, L.F. Bonewald, Effect of bioactive

borate glass microstructure on bone regeneration, angiogenesis, and hydroxyapatite conversion in a rat calvarial defect model, Acta Biomater. 9 (2013) 8015–8026. https://doi.org/10.1016/j.actbio.2013.04.043.

[57] L. Bi, S. Jung, D. Day, K. Neidig, V. Dusevich, D. Eick, L. Bonewald, Evaluation of bone regeneration, angiogenesis, and hydroxyapatite conversion in critical-sized rat calvarial defects implanted with bioactive glass scaffolds, J. Biomed. Mater. Res. Part A. 100A (2012) 3267–3275. https://doi.org/10.1002/jbm.a.34272.

[58] O.N. Chupakhin, T.G. Khonina, N. V. Kungurov, N. V. Zilberberg, N.P. Evstigneeva, M.M. Kokhan, A.I. Polishchuk, E. V. Shadrina, E.Y.L. Larchenko, L.P. Larionov, M.S. Karabanalov, Silicon–boron containing glycerohydrogel having wound healing, regenerative, and antimicrobial activity, Russ. Chem. Bull. Int. Ed. 66 (2017) 558–563.

[59] Y. Lin, W. Xiao, B. Sonny Bal, M.N. Rahaman, Effect of copper-doped silicate 13–93 bioactive glass scaffolds on the response of MC3T3-E1 cells in vitro and on bone regeneration and angiogenesis in rat calvarial defects in vivo, Mater. Sci. Eng. C. 67 (2016) 440–452. https://doi.org/10.1016/j.msec.2016.05.073.

[60] C. Gérard, L. Bordeleau, J. Barralet, C.J. Doillon, The stimulation of angiogenesis and collagen deposition by copper, Biomaterials. 31 (2010) 824–831. https://doi.org/10.1016/j.biomaterials.2009.10.009.

[61] N. Mroczek-Sosnowska, E. Sawosz, K.P. Vadalasetty, M. Łukasiewicz, J. Niemiec, M. Wierzbicki, M. Kutwin, S. Jaworski, A. Chwalibog, Nanoparticles

of copper stimulate angiogenesis at systemic and molecular level, Int. J. Mol. Sci. 16 (2015) 4838–4849. https://doi.org/10.3390/ijms16034838.

[62] C. Wu, Y. Zhou, M. Xu, P. Han, L. Chen, J. Chang, Y. Xiao, Copper-containing mesoporous bioactive glass scaffolds with multifunctional properties of angiogenesis capacity, osteostimulation and antibacterial activity, Biomaterials. 34 (2013) 422–433. https://doi.org/10.1016/j.biomaterials.2012.09.066.

[63] K.J. Woo, C.K. Hye, W.K. Ki, S. Shin, H.K. So, H.P. Yong, Antibacterial activity and mechanism of action of the silver ion in Staphylococcus aureus and Escherichia coli, Appl. Environ. Microbiol. 74 (2008) 2171–2178. https://doi.org/10.1128/AEM.02001-07.

[64] M. Bellantone, H.D. Williams, L.L. Hench, Broad-spectrum bactericidal activity of Ag2O-doped bioactive glass, Antimicrob. Agents Chemother. 46 (2002) 1940–1945. https://doi.org/10.1128/AAC.46.6.1940.

[65] A. Bari, N. Bloise, S. Fiorilli, G. Novajra, M. Vallet-Regí, G. Bruni, A. Torres-Pardo, J.M. González-Calbet, L. Visai, C. Vitale-Brovarone, Copper-containing mesoporous bioactive glass nanoparticles as multifunctional agent for bone regeneration, Acta Biomater. 55 (2017) 493–504. https://doi.org/10.1016/j.actbio.2017.04.012.

[66] G. Applerot, J. Lellouche, A. Lipovsky, Y. Nitzan, R. Lubart, A. Gedanken, E. Banin, Understanding the antibacterial mechanism of CuO nanoparticles: Revealing the route of induced oxidative stress, Biomed. Mater. 8 (2012) 3326–3337. https://doi.org/10.1002/smll.201200772.

[67] E. Kulczycki, D.A. Fowle, P.A. Kenward, K. Leslie, W. David, G. Roberts, J.A. Roberts, Stimulation of methanotroph activity by Cu- substituted borosilicate glass, Geomicrobiol. J. 28 (2011) 1–10. https://doi.org/10.1080/01490451003614971.

[68] J.M.P. Almeida, L. De Boni, W. Avansi, C. Ribeiro, E. Longo, A.C. Hernandes, C.R. Mendonca, Generation of copper nanoparticles induced by fs-laser irradiation in borosilicate glass, Opt. Express. 20 (2012) 15106–15113.

[69] H. Wang, S. Zhao, W. Xiao, J. Xue, Y. Shen, J. Zhou, W. Huang, C. Rahaman, Mohamed N. Zhang, D. Wang, Influence of Cu doping in borosilicate bioactive glass and the properties of its derived scaffolds, Mater. Sci. Eng. C. 58 (2016) 194–203. https://doi.org/10.1016/j.msec.2015.08.027.

[70] E. Meechoowas, M. Müller, C. Rüssel, Redox relaxation in a sodium borosilicate glass doped with copper and arsenic, antimony, or tin, J. Non. Cryst. Solids. 356 (2010) 2528–2533. https://doi.org/10.1016/j.jnoncrysol.2010.03.034.

[71] S. Shailajha, K. Geetha, P. Vasantharani, S.P.S. Abdul, Effects of copper on the preparation and characterization of Na–Ca–P borate glasses, Spectrochim. Acta Part A Mol. Biomol. Spectrosc. 138 (2015) 846–856. https://doi.org/10.1016/j.saa.2014.10.101.

[72] D. Möncke, E.I. Kamitsos, D. Palles, R. Limbach, A. Winterstein-Beckmann, T. Honma, Z. Yao, T. Rouxel, L. Wondraczek, Transition and post-transition metal ions in borate glasses: Borate ligand speciation, cluster formation, and their effect on glass transition and mechanical properties, J. Chem. Phys. 145 (2017)

124501–124516. https://doi.org/10.1063/1.4962323.

[73] K.H. Obayes, H. Wagiran, R. Hussin, M.A. Saeed, A new strontium/copper co-doped lithium borate glass composition with improved dosimetric features, J. Lumin. 176 (2016) 202–211. https://doi.org/10.1016/j.jlumin.2016.03.024.

[74] M. Miglierini, M. Hasiak, M. Bujdoš, Subsurface structure and magnetic parameters of Fe-Mo-Cu-B metallic glass, Nukleonika. 60 (2015) 115–119. https://doi.org/10.1515/nuka-2015-0023.

[75] Z.Y. Yao, D. Möncke, E.I. Kamitsos, P. Houizot, F. Célarié, T. Rouxel, L. Wondraczek, Structure and mechanical properties of copper–lead and copper–zinc borate glasses, J. Non. Cryst. Solids. 435 (2016) 55–68. https://doi.org/10.1016/j.jnoncrysol.2015.12.005.

[76] K. Schuhladen, X. Wang, L. Hupa, A.R. Boccaccini, Dissolution of borate and borosilicate bioactive glasses and the influence of ion (Zn, Cu) doping in different solutions, J. Non. Cryst. Solids. 502 (2018) 22–34. https://doi.org/10.1016/j.jnoncrysol.2018.08.037.

[77] G.J. Owens, R.K. Singh, F. Foroutan, M. Alqaysi, C.-M. Han, C. Mahapatra, H.-W. Kim, J.C. Knowles, Sol–gel based materials for biomedical applications, Prog. Mater. Sci. 77 (2016) 1–79. https://doi.org/10.1016/j.pmatsci.2015.12.001.

[78] K. Zheng, A.R. Boccaccini, Sol-gel processing of bioactive glass nanoparticles: A review, Adv. Colloid Interface Sci. 249 (2017) 363–373. https://doi.org/10.1016/j.cis.2017.03.008.

[79] L.P. Singh, S.K. Bhattacharyya, R. Kumar, G. Mishra, U. Sharma, G. Singh, S. Ahalawat, Sol-Gel processing of silica nanoparticles and their applications, Adv. Colloid Interface Sci. 214 (2014) 17–37. https://doi.org/10.1016/j.cis.2014.10.007.

[80] A.E. Danks, S.R. Hall, Z. Schnepp, The evolution of 'sol–gel' chemistry as a technique for materials synthesis, Mater. Horizons. 3 (2016) 91–112. https://doi.org/10.1039/c5mh00260e.

[81] F. Baino, E. Fiume, M. Miola, E. Verné, Bioactive sol-gel glasses: Processing, properties, and applications, Appl. Ceram. Technol. 15 (2018) 841–860. https://doi.org/10.1111/ijac.12873.

[82] S. Kargozar, F. Baino, N. Lotfibakhshaiesh, R.G. Hill, P.B. Milan, S. Hamzehlou, M.T. Joghataei, M. Mozafari, When size matters: Biological response to strontium- and cobalt- substituted bioactive glass particles, Mater. Today Proc. 5 (2018) 15768–15775. https://doi.org/10.1016/j.matpr.2018.04.190.

[83] A.A.R. de Oliveira, D.A. de Souza, L.L. Silveira Dias, S.M. de Carvalho, H.S. Mansur, M. de Magalhaes Pereira, Synthesis, characterization and cytocompatibility of spherical bioactive glass nanoparticles for potential hard tissue engeering applications, Biomed. Mater. 8 (2013) 1–14. https://doi.org/10.1088/1748-6041/8/2/025011.

[84] F. Bonino, A. Damin, V. Aina, M. Miola, E. Verné, O. Bretcanu, S. Bordiga, A. Zecchina, C. Morterra, In situ Raman study to monitor bioactive glasses reactivity, J. Raman Spectrosc. 39 (2008) 260–264. https://doi.org/10.1002/jrs.

[85] C. Vichery, J.-M. Nedelec, Bioactive glass nanoparticles: from synthesis to materials design for biomedical applications, Materials. 9 (2016) 1–17. https://doi.org/10.3390/ma9040288.

[86] A. Lukowiak, J. Lao, J. Lacroix, J.-M. Nedelec, Bioactive glass nanoparticles obtained through sol–gel chemistry, Chemmical Commun. 49 (2013) 6620–6622. https://doi.org/10.1039/c3cc00003f.

[87] S.L. Greasley, S.J. Page, S. Sirovica, S. Chen, R.A. Martin, A. Riveiro, J. V Hanna, A.E. Porter, J.R. Jones, Controlling particle size in the Stöber process and incorporation of calcium, J. Colloid Interface Sci. 469 (2016) 213–223. https://doi.org/10.1016/j.jcis.2016.01.065.

[88] W. Stöber, A. Fink, Controlled growth of monodisperse silica spheres in the micron size range, J. Colloid Interface Sci. 26 (1968) 62–69.

[89] G.M. Luz, J.F. Mano, Nanoengineering of bioactive glasses: hollow and dense nanospheres, J. Nanoparticle Res. 15 (2013) 1–11. https://doi.org/10.1007/s11051-013-1457-0.

[90] B. Topuz, D. Şimşek, M. Çiftçioğlu, Preparation of monodisperse silica spheres and determination of their densification behaviour, Ceram. Int. 41 (2015) 43–52. https://doi.org/10.1016/j.ceramint.2014.07.112.

[91] Q. Guo, D. Huang, X. Kou, W. Cao, L. Li, L. Ge, J. Li, Synthesis of disperse amorphous SiO2 nanoparticles via sol–gel process, Ceram. Int. 43 (2017) 192–196. https://doi.org/10.1016/j.ceramint.2016.09.133.

[92] F. Branda, B. Silvestri, G. Luciani, A. Costantini, The effect of mixing alkoxides on the Stöber particles size, Colloids Surfaces A Physiochemistry Eng. Asp. 299 (2007) 252–255. https://doi.org/10.1016/j.colsurfa.2006.11.048.

[93] W. Xia, J. Chang, Preparation and characterization of nano-bioactive-glasses (NBG) by a quick alkali-mediated sol–gel method, Mater. Lett. 61 (2007) 3251–3253. https://doi.org/10.1016/j.matlet.2006.11.048.

[94] V. Aina, F. Bonino, C. Morterra, M. Miola, C.L. Bianchi, G. Malavasi, M. Marchetti, V. Bolis, Influence of the chemical composition on nature and activity of the surface layer of Zn-substituted Sol-Gel (bioactive) glasses, J. Phys. Chem. C. 115 (2011) 2196–2210. https://doi.org/10.1021/jp1101708.

[95] Z.-A. Qiao, L. Zhang, M. Guo, Y. Liu, Q. Huo, Synthesis of mesoporous silica nanoparticles via controlled hydrolysis and condensation of silicon alkoxide, Chem. Mater. 21 (2009) 3823–3829. https://doi.org/10.1021/cm901335k.

[96] M. Magallanes-Perdomo, S. Meille, J.-M. Chenal, E. Pacard, J. Chevalier, Bioactivity modulation of Bioglass ® powder by thermal treatment, J. Eur. Ceram. Soc. 32 (2012) 2765–2775. https://doi.org/10.1016/j.jeurceramsoc.2012.03.018.

[97] Z. Hong, A. Liu, L. Chen, X. Chen, X. Jing, Preparation of bioactive glass ceramic nanoparticles by combination of sol–gel and coprecipitation method, J. Non. Cryst. Solids. 355 (2009) 368–372. https://doi.org/10.1016/j.jnoncrysol.2008.12.003.

[98] E.M.F. Lemos, S.M. Carvalho, P.S.O. Patrício, C.L. Donnici, M.M. Pereira,

Comparison of the effect of sol-gel and coprecipitation routes on the properties and behavior of nanocomposite chitosan-bioactive glass membranes for bone tissue engineering, J. Nanomater. 2015 (2015) 1–8.

[99] Y.-F. Goh, A.Z. Alshemary, M. Akram, A.R.M. Kadir, R. Hussain, Bioactive glass: An in-vitro comparative study of doping with nanoscale copper and silver particles, Int. J. Appl. Glas. Sci. 266 (2014) 255–266. https://doi.org/10.1111/ijag.12061.

[100] L.M. Mukundan, R. Nirmal, D. Vaikkath, P.D. Nair, A new synthesis route to high surface area sol gel bioactive glass through alcohol washing: A preliminary study, Biomatter. 3 (2013) 24288–24291. https://doi.org/10.4161/biom.24288.

[101] J.P. Fan, P. Kalia, L. Di Silvio, J. Huang, In vitro response of human osteoblasts to multi-step sol-gel derived bioactive glass nanoparticles for bone tissue engineering, Mater. Sci. Eng. C. 36 (2014) 206–214. https://doi.org/10.1016/j.msec.2013.12.009.

[102] J. Ajita, S. Saravanan, N. Selvamurugan, Effect of size of bioactive glass nanoparticles on mesenchymal stem cell proliferation for dental and orthopedic applications, Mater. Sci. Eng. C. 53 (2015) 142–149. https://doi.org/10.1016/j.msec.2015.04.041.

[103] V. Mortazavi, M.M. Nahrkhalaji, M.H. Fathi, S.B. Mousavi, B.N. Esfahani, Antibacterial effects of sol-gel-derived bioactive glass nanoparticle on aerobic bacteria, J. Biomed. Mater. Res. A. 94 (2010) 160–168. https://doi.org/10.1002/jbm.a.32678.

[104] S. Chen, A. Osaka, S. Hayakawa, K. Tsuru, E. Fujii, K. Kawabata, Microstructure evolution in Stöber-type silica nanoparticles and their in vitro apatite deposition, J. Sol-Gel Sci. Technol. 48 (2008) 322–335. https://doi.org/10.1007/s10971-008-1823-z.

[105] S. Zhao, Y. Li, D. Li, Synthesis and in vitro bioactivity of CaO–SiO2–P2O5 mesoporous microspheres, Microporous Mesoporous Mater. 135 (2010) 67–73. https://doi.org/10.1016/j.micromeso.2010.06.012.

[106] N. Gupta, D. Santhiya, S. Murugavel, A. Kumar, A. Aditya, M. Ganguli, S. Gupta, Effects of transition metal ion dopants (Ag, Cu and Fe) on the structural, mechanical and antibacterial properties of bioactive glass, Colloids Surfaces A. 538 (2018) 393–403. https://doi.org/10.1016/j.colsurfa.2017.11.023.

[107] C. Wu, R. Miron, A. Sculean, S. Kaskel, T. Doert, R. Schulze, Y. Zhang, Proliferation, differentiation and gene expression of osteoblasts in boron-containing associated with dexamethasone deliver from mesoporous bioactive glass scaffolds, Biomaterials. 32 (2011) 7068–7078. https://doi.org/10.1016/j.biomaterials.2011.06.009.

[108] H. Luo, J. Xiao, M. Peng, Q. Zhang, Z. Yang, H. Si, One-pot synthesis of copper-doped mesoporous bioglass towards multifunctional 3D nano fibrous scaffolds for bone regeneration, J. Non. Cryst. Solids. 532 (2020). https://doi.org/10.1016/j.jnoncrysol.2019.119856.

[109] K. Zheng, E. Torre, A. Bari, N. Taccardi, C. Cassinelli, M. Morra, S. Fiorilli, C. Vitale-Brovarone, G. Iviglia, A.R. Boccaccini, Antioxidant mesoporous Ce-

doped bioactive glass nanoparticles with anti-inflammatory and pro-osteogenic activities, Mater. Today Bio. 5 (2020) 1–14. https://doi.org/10.1016/j.mtbio.2020.100041.

[110] A.M. El-Kady, M.M. Ahmed, B.M.A. El-Hady, A.F. Ali, A.M. Ibrahim, Optimization of ciprofloxacin release kinetics of novel nano-bioactive glasses: Effect of glass modifier content on drug loading and release mechanism, J. Non. Cryst. Solids. 521 (2019) 1–12. https://doi.org/10.1016/j.jnoncrysol.2019.119471.

[111] X. Kesse, C. Vichery, J.-M. Nedelec, Deeper insights into a bioactive glass nanoparticle synthesis protocol to control its morphology, dispersibility , and composition, ACS Omega. 4 (2019) 5768–5775. https://doi.org/10.1021/acsomega.8b03598.

[112] W. Yu, K. Sepehrnoori, Modeling gas adsorption in Marcellus shale using Langmuir and BET isotherms, in: Shale Gas Tight Oil Reserv. Simul., 2018: pp. 129–154. https://doi.org/10.1016/b978-0-12-813868-7.00004-3.

[113] K.A. Cychosz, M. Thommes, Progress in the physisorption characterization of nanoporous gas storage materials, Engineering. 4 (2018) 559–566. https://doi.org/10.1016/j.eng.2018.06.001.

[114] P. Sepulveda, J.R. Jones, L.L. Hench, Characterization of melt-derived 45S5 and sol-gel–derived 58S bioactive glasses, J. Biomed. Mater. Res. 58 (2001) 734–740. https://doi.org/10.1002/jbm.0000.

[115] Q. Hu, Y. Li, N. Zhao, C. Ning, X. Chen, Facile synthesis of hollow mesoporous bioactive glass sub-micron spheres with a tunable cavity size, Mater. Lett. 134

(2014) 130–133. https://doi.org/10.1016/j.matlet.2014.07.041.

[116] G. Miao, X. Chen, H. Dong, L. Fang, C. Mao, Y. Li, Investigation of emulsified, acid and acid-alkali catalyzed mesoporous bioactive glass microspheres for bone regeneration and drug delivery, Mater. Sci. Eng. C. 33 (2013) 4236–4243. https://doi.org/10.1016/j.msec.2013.06.022.

[117] M. Catauro, A. Dell, S. Vecchio, Synthesis, structural, spectroscopic and thermoanalytical study of sol–gel derived SiO2–CaO–P2O5 gel and ceramic materials, Thermochim. Acta. 625 (2016) 20–27. https://doi.org/10.1016/j.tca.2015.12.004.

[118] D. Moura, M.T. Souza, L. Liverani, G. Rella, G.M. Luz, J.F. Mano, A.R. Boccaccini, Development of a bioactive glass-polymer composite for wound healing applications, Mater. Sci. Eng. C. 76 (2017) 224–232. https://doi.org/10.1016/j.msec.2017.03.037.

[119] T. Mantsos, X. Chatzistavrou, J.A. Roether, L. Hupa, H. Arstila, A.R. Boccaccini, Non-crystalline composite tissue engineering scaffolds using boron-containing bioactive glass and poly (D, L-lactic acid) coatings, Biomed. Mater. 4 (2009) 1–12. https://doi.org/10.1088/1748-6041/4/5/055002.

[120] M. Mozafari, F. Moztarzadeh, M. Tahriri, Investigation of the physico-chemical reactivity of a mesoporous bioactive SiO2–CaO–P2O5 glass in simulated body fluid, J. Non. Cryst. Solids. 356 (2010) 1470–1478. https://doi.org/10.1016/j.jnoncrysol.2010.04.040.

[121] H. Yin, C. Yang, Y. Gao, C. Wang, M. Li, H. Guo, Q. Tong, Fabrication and

characterization of strontium-doped borate-based bioactive glass scaffolds for bone tissue engineering, J. Alloys Compd. 743 (2018) 564–569. https://doi.org/10.1016/j.jallcom.2018.01.099.

[122] I. Kashif, A. Ratep, Role of copper metal or oxide on physical properties of lithium borate glass, J. Mol. Struct. 1102 (2015) 1–5. https://doi.org/10.1016/j.molstruc.2015.07.070.

[123] H. Doweidar, G. El-Damrawi, M. Al-Zaibani, Distribution of species in Na2O-CaO–B2O3 glasses as probed by FTIR, Vib. Spectrosc. 68 (2013) 91–95. https://doi.org/10.1016/j.vibspec.2013.05.015.

[124] E.E. Horopanitis, G. Perentzis, A. Beck, L. Guczi, G. Peto, L. Papadimitriou, Identification of the presence of crystalline phase in lithiated boron oxide ionic glass conductors, Mater. Sci. Eng. B. 165 (2009) 156–159. https://doi.org/10.1016/j.mseb.2009.09.015.

[125] W.C. Lepry, S.N. Nazhat, Highly Bioactive Sol-Gel-Derived Borate Glasses, Chem. Mater. 27 (2015) 4821–4831. https://doi.org/10.1021/acs.chemmater.5b01697.

[126] H.E. Çamurlu, E. Akarsu, O. Arslan, S. Mathur, Nanocomposite glass coatings containing hexagonal boron nitride nanoparticles, Ceram. Int. 42 (2016) 8856–8862. https://doi.org/10.1016/j.ceramint.2016.02.133.

[127] A.A. Zadpoor, Relationship between in vitro apatite-forming ability measured using simulated body fluid and in vivo bioactivity of biomaterials, Mater. Sci. Eng. C. 35 (2014) 134–143. https://doi.org/10.1016/j.msec.2013.10.026.

[128] A.J. Salinas, M. Vallet-Regí, I. Izquierdo-Barba, Biomimetic apatite deposition on calcium silicate gel glasses, J. Sol-Gel Sci. Technol. 21 (2001) 13–25.

[129] M. Catauro, F. Papale, L. Sapio, S. Naviglio, Biological influence of Ca/P ratio on calcium phosphate coatings by sol-gel processing, Mater. Sci. Eng. C. 65 (2016) 188–193. https://doi.org/10.1016/j.msec.2016.03.110.

[130] T. Shimogaki, H. Tokoro, M. Tabuchi, N. Koike, Y. Yamashina, M. Takahashi, Large-scale synthesis of monodisperse microporous silica nanoparticles by gradual injection of reactants, J. Sol-Gel Sci. Technol. 74 (2015) 109–113. https://doi.org/10.1007/s10971-014-3583-2.

[131] R.M. Rad, A.Z. Alshemary, Z. Evis, D. Keskin, K. Altunbas, A. Tezcaner, K. Altunba, A. Tezcaner, Structural and biological assessment of boron doped bioactive glass nanoparticles for dental tissue applications, Ceram. Int. 44 (2018) 9854–9864. https://doi.org/10.1016/j.ceramint.2018.02.230.

[132] Y. Zhang, J. Luan, S. Jiang, X. Zhou, M. Li, The effect of amino-functionalized mesoporous bioactive glass on MC3T3-E1 cells in vitro stimulation, Compos. Part B. 172 (2019) 397–405. https://doi.org/10.1016/j.compositesb.2019.05.104.

[133] A. Lardner, The effects of extracellular pH on immune function, J. Leukoc. Biol. 69 (2001) 522–30. https://doi.org/10.1189/jlb.69.4.522.

[134] C. de Vallière, S. Vida, I. Clay, G. Jurisic, I. Tcymbarevich, S. Lang, M.G. Ludwig, M. Okoniewski, J.J. Eloranta, G.A. Kullak-Ublick, C.A. Wagner, G. Rogler, K. Seuwen, The pH-sensing receptor OGR1 improves barrier function of epithelial cells and inhibits migration in an acidic environment, Am. J. Physiol. -

Gastrointest. Liver Physiol. 309 (2015) 475–490. https://doi.org/10.1152/ajpgi.00408.2014.

[135] M. Araújo, M. Miola, G. Baldi, J. Perez, E. Verné, Bioactive glasses with low Ca/P ratio and enhanced bioactivity, Materials. 9 (2016). https://doi.org/10.3390/ma9040226.

[136] J. Bejarano, P. Caviedes, H. Palza, Sol–gel synthesis and in vitro bioactivity of copper and zinc-doped silicate bioactive glasses and glass-ceramics, Biomed. Mater. 10 (2015) 1–13. https://doi.org/10.1088/1748-6041/10/2/025001.

[137] X. Li, J. Shi, X. Dong, L. Zhang, H. Zeng, A mesoporous bioactive glass / polycaprolactone composite scaffold and its bioactivity behavior, J. Biomed. Mater. Res. Part A. 84 (2007) 84–91. https://doi.org/10.1002/jbm.a.

[138] V. Miguez-Pacheco, D. de Ligny, J. Schmidt, R. Detsch, A.R. Boccaccini, Development and characterization of niobium-releasing silicate bioactive glasses for tissue engineering applications, J. Eur. Ceram. Soc. 38 (2018) 871–876. https://doi.org/10.1016/j.jeurceramsoc.2017.07.028.